THE ASTROPHYSICAL JOURNAL SUPPLEMENT SERIES, 149:29–51, 2003 November

THE *ROSAT* NORTH ECLIPTIC POLE SURVEY: THE OPTICAL IDENTIFICATIONS

I. M. GIOIA[1]
Istituto di Radioastronomia del CNR, Via Gobetti 101, I-40129 Bologna, Italy; and Institute for Astronomy, University of Hawai'i

J. P. HENRY[1]
Institute for Astronomy, University of Hawai'i, 2680 Woodlawn Drive, Honolulu, HI 96822

C. R. MULLIS[1]
European Southern Observatory, Karl-Schwarzschildstrasse 2, Garching bei München D-85740, Germany; and Institute for Astronomy, University of Hawai'i

H. BÖHRINGER, U. G. BRIEL, AND W. VOGES
Max-Planck-Institut fur Extraterrestrische Physik, Giessenbachstrasse, Postfach 1312, Garching D-85741, Germany

AND

J. P. HUCHRA[2]
Harvard-Smithsonian Center for Astrophysics, 60 Garden Street, Cambridge, MA 02138
Received 2003 March 28; accepted 2003 July 3

ABSTRACT

The X-ray data around the North Ecliptic Pole (NEP) of the *ROSAT* All Sky Survey have been used to construct a contiguous area survey consisting of a sample of 445 individual X-ray sources above a flux of $\sim 2 \times 10^{-14}$ ergs cm^{-2} s^{-1} in the 0.5–2.0 keV energy band. The NEP survey is centered at $\alpha_{2000} = 18^{\rm h}00^{\rm m}$, $\delta_{2000} = +66°33'$ and covers a region of 80.7 deg^2 at a moderate Galactic latitude of $b = 29\overset{\circ}{.}8$. Hence, the NEP survey is as deep and covers a comparable solid angle to the *ROSAT* serendipitous surveys but is also contiguous. We have identified 99.6% of the sources and determined redshifts for the extragalactic objects. In this paper we present the optical identifications of the NEP catalog of X-ray sources including basic X-ray data and properties of the sources. We also describe with some detail the optical identification procedure. The classification of the optical counterparts to the NEP sources is very similar to that of previous surveys, in particular the *Einstein* Extended Medium Sensitivity Survey (EMSS). The main constituents of the catalog are active galactic nuclei (AGNs) (~49%), either type 1 or type 2 according to the broadness of their permitted emission lines. Stellar counterparts are the second most common identification class (~34%). Clusters and groups of galaxies comprise 14%, and BL Lacertae objects 2%. One non-AGN galaxy and one planetary nebula have also been found. The NEP catalog of X-ray sources is a homogeneous sample of astronomical objects featuring complete optical identification.

Subject headings: BL Lacertae objects: general — catalogs — galaxies: clusters: general — surveys — X-rays: general — X-rays: stars

On-line material: machine-readable table

1. INTRODUCTION

Since their appearance in the 1970s, X-ray surveys played the major role in our understanding of the X-ray universe. The goals of these surveys are to provide a detailed accounting of the classes of discrete sources that make up the X-ray sky, and also to define large, complete samples of X-ray selected objects for statistical and individual studies. Statistical analyses of flux-limited and optically identified samples of astronomical objects supply important information on quantities such as source counts, luminosity functions, cosmological evolution, and X-ray background contributions of the different populations. Clusters of galaxies are a class of X-ray sources in which we are particularly interested as they are important probes for the evolution of cosmic structure and for the test of cosmological models (Gioia et al. 2001). The advantage to construct cluster samples for cosmological studies from X-ray surveys is the more direct relation between luminosity and mass. The derived X-ray luminosity function is closely related to the mass function of the clusters, which is used as an important calibrator of the amplitude of the density fluctuation power spectrum. The first X-ray imaging instruments on board the *Einstein Observatory* allowed the construction of the EMSS catalogs of active galactic nuclei (AGNs), galaxy clusters, BL Lac objects, and stars (Gioia et al. 1990b; Stocke et al. 1991; Maccacaro et al. 1994) and the discovery of the negative evolution of the space density of X-ray clusters (Gioia et al. 1990a; Henry et al. 1992). Given the diverse nature of the X-ray emission from the various X-ray counterparts (e.g., diffuse hot cluster gas, nonthermal AGN emission, and stellar coronae) a variety of complementary observations were required to correctly identify the optical objects associated with the EMSS X-ray sources. The EMSS was constructed using those objects found serendipitously

[1] Visiting Astronomer at Canada-France-Hawai'i Telescope, operated by the National Research Council of Canada, le Centre National de la Recherche Scientifique de France and the University of Hawai'i, and at the W. M. Keck Observatory, jointly operated by the California Institute of Technology, the University of California, and the National Aeronautics and Space Administration.

[2] Observations reported here were made at the Multiple Mirror Telescope Observatory, a joint facility of the Smithsonian Institution and the University of Arizona.

in each field after excluding the central region of the field including the target itself.

ROSAT (Trümper 1983) was the first X-ray imaging experiment to survey the entire sky. After its launch a greatly increased sensitivity and source location accuracy over all previous X-ray sky surveys were available. Many X-ray surveys were compiled either from the *ROSAT* All-Sky-Survey data (RASS; Voges et al. 1999) or from pointed data (i.e., EMSS-like surveys, but mostly to search for clusters of galaxies). In general, the surveys extracted from the RASS, the contiguous area surveys, cover a very large solid angle ($\sim$10,000 deg^2 or more) but are shallower than the pointed data surveys. Given the large solid angle sampled and the sizes of the superstructures (several hundreds of Mpc), the contiguous area surveys, and in particular the all sky surveys, are good tracers of large-scale structure. They allow investigations of the clustering properties of clusters and of the power spectrum of their distribution. The contiguous area surveys typically sample the nearby universe ($z < 0.3$) and are used as an excellent local reference for cluster studies at higher redshift. Among the contiguous area surveys we mention the BCS (Ebeling et al. 1998), and its extension eBCS (Ebeling et al. 2000), RASS1-BS (De Grandi et al. 1999), NORAS (Böhringer et al. 2000), MACS (Ebeling, Edge, & Henry 2001), REFLEX (Böhringer et al. 2001), and the NEP survey (Mullis 2001; Henry et al. 2001; Voges et al. 2001).

The great advantage of the serendipitous surveys, those extracted from the pointed data, is their much higher sensitivity, about 2 orders of magnitude deeper than the contiguous area surveys ($\sim 10^{-14}$ vs. $\sim 10^{-12}$ ergs cm^{-2} s^{-1} in the *ROSAT* band), even though their solid angle is less than $\sim$200 deg^2. The serendipitous surveys are not restricted to the local universe but probe $z > 4$ for quasars and $z > 1$ for clusters of galaxies. As with the contiguous area surveys, many sources are common to the serendipitous surveys since all use the same pointed *ROSAT* data (see Table 5 in Mullis et al. 2003, for common cluster sources in all the present X-ray surveys). Among the serendipitous X-ray surveys for clusters of galaxies we mention the RDCS (Rosati et al. 1995, 1998), RIXOS (Castander et al. 1995; Mason et al. 2000), Southern SHARC (Burke et al. 1997; Collins et al. 1997), Bright SHARC (Romer et al. 2000), 160 deg^2 (Vikhlinin et al. 1998; Mullis et al. 2003), WARPS (Perlman et al. 2002 and references therein), BMW (Campana et al. 1999; Lazzati et al. 2001), and ROXS (Donahue et al. 2002).

We have used data around the North Ecliptic Pole of the RASS to construct a contiguous area survey consisting of a homogeneous sample of 445 X-ray sources. The region around the NEP possesses the deepest exposure and consequently the greatest sensitivity of the entire RASS. Hence, the $9° \times 9°$ survey region centered at $\alpha_{2000} = 18^{\rm h}00^{\rm m}$, $\delta_{2000} = +66°33'$ covers the deepest, wide-angle contiguous region ever observed in X-rays. This unique combination of depth plus wide, contiguous solid angle provides the capabilities of detecting both high-redshift objects and large-scale structure, which were the aims of our involvement in the survey.

A comprehensive description of the *ROSAT* NEP Survey and the principal results are presented in Mullis (2001).[3] An overview of the NEP survey, including the selection function, the optical identification program, and number-count distributions for the various classes of objects, has been published in Henry et al. (2001). Voges et al. (2001) gives a summary of the X-ray data and the statistical properties of the NEP sources. Gioia et al. (2001) present evidence for cluster X-ray luminosity evolution, and Mullis et al. (2001) describe the details on the NEP supercluster found in the survey X-ray data. In this paper we discuss in more detail the optical identification program and the methodology used to identify the sources, and we present the optical catalog with a description of the optical properties of the sources. For convenience, we give the basic X-ray properties of the sources, but a more detailed description of the X-ray data, the detection algorithm, and the statistical properties of the NEP sources will appear in a subsequent paper. For consistency with previous work, we assume throughout the paper a Hubble constant of $H_0 = 50\ h_{50}$ km s^{-1} Mpc^{-1}, a matter density parameter $\Omega_{M0} = 1$, and a cosmological constant of $\Omega_{\Lambda 0} = 0$.

[3] A link to his thesis can be found at http://www.ifa.hawaii.edu/~mullis/nep-phd.html.

2. THE X-RAY DATA

The NEP region was observed many times by the *ROSAT* satellite since the RASS scan pattern overlapped at the ecliptic poles. While the mean RASS exposure time across the entire sky is approximately 400 s, the NEP region exposure time approaches 40 ks at the pole. The minimum, median, and maximum exposure times in the NEP survey regions are 1.7, 4.8, and 38 ks, respectively. The 80.7 deg^2 NEP region is a good area to pursue unbiased surveys of the extragalactic sky since it is at a moderate Galactic latitude of $b = 29\overset{\circ}{.}8$ ($l = 96\overset{\circ}{.}4$) and has a mean neutral column density of $\langle n_{\rm H} \rangle \approx 4.3 \times 10^{20}$ cm^{-2} (Elvis, Lockmann, & Fassnacht 1994). The other pole of the ecliptic where the exposure is piling up, the South Ecliptic Pole region, or SEP, has much less exposure since the PSPC was automatically shut off because of the enhanced charged particle density of the South Atlantic Anomalies, which could damage the detector. Furthermore, the SEP is in the vicinity of the Large Magellanic Clouds, a crowded stellar region that is not amenable for extragalactic work. All of these considerations make the NEP survey unique.

The data used in our work were extracted from the second processing of the *ROSAT* data (RASS-II), which has improved attitude quality, improved spline-fitted background map, and fully merged photon data (Voges et al. 1999). The detection algorithm of the RASS is based on a multiscale, sliding detect aperture (Voges et al. 1999). Candidate sources identified by this procedure, operating at a low acceptance threshold, were passed to a maximum-likelihood (ML) algorithm for more accurate determinations of source existence likelihood and other interesting parameters (Voges et al. 2001; Mullis 2001).

To be part of the NEP survey an X-ray source must be in the right ascension range $17^{\rm h}15^{\rm m} < \alpha_{2000} < 18^{\rm h}45^{\rm m}$ and in the declination range $62° < \delta_{2000} < 71°$; its maximum likelihood of existence must be $L \geq 10$, where $L = -\ln P$ and P is the probability that the source count rate is zero; its signal-to-noise ratio for source count rate must be greater than 4 σ. The detection energy band used is the *ROSAT* broadband 0.1–2.4 keV. There are 445 unique sources within the survey region fulfilling these requirements. Twenty-one multidetections of individual, often extended, sources were removed in constructing the final sample. Approximately 2 of the 445 sources are expected to be spurious considering the survey solid angle and telescope beam size appropriate for the RASS (half-power diameter $=3\farcm1$; Boese 2000). Of the 515 additional X-ray sources with a likelihood of existence $L < 10$ in the NEP region, only three have a signal-to-noise ratio of more than 4 σ. Hence, the principal selection criterion for the NEP survey is the 4 σ threshold in count rate significance.

The observed count rate for each source is extracted from a $5'$ radius circular aperture (except for one source, RX J1834.1+7057, where $r_{\rm extract} = 6\farcm5$). Different model spectra, according to the source nature, have been adopted to convert from count rates to detect flux. An additional correction is applied to the detect flux of extragalactic X-ray sources to account for the effect of Galactic absorption along the line of sight. Unabsorbed fluxes were derived using neutral hydrogen ($n_{\rm H}$) column density data obtained from the 21 cm observations of Elvis et al. (1994), supplemented by Stark, Gammie, & Wilson (1992), at the location of the X-ray source. The minimum, median, and maximum neutral $n_{\rm H}$ for the NEP sources are (2.4, 4.2, 8.2) $\times 10^{20}$ cm^{-2}, respectively.

For AGNs we have used a power-law spectrum with an energy index of -1, resulting in a median conversion factor from count rate (0.1–2.4 keV) to flux (0.5–2.0 keV) of 1.20×10^{-11}, with a $\pm 12\%$ variation over the full range of column densities sampled by the NEP AGNs. For galaxy clusters a Raymond-Smith plasma spectrum was adopted, with a metallicity of 0.3 solar plus a plasma temperature, and a measured redshift particular to each cluster. The gas temperature of the intracluster medium is estimated using the $L_{\rm X}$-kT relation of White, Jones, & Forman (1997), $kT = 2.76$ keV $L_{\rm X,bol,44}^{0.33}$, where $L_{\rm X,bol,44}^{0.33}$ is the bolometric X-ray luminosity in units of 10^{44} ergs s^{-1}. An iterative process begins by assuming a temperature of 5 keV. Total flux is converted to a K-corrected luminosity[4] in the 0.5–2.0 keV band, which is converted to a bolometric luminosity. This preliminary $L_{\rm X,bol,44}$ is used to predict the cluster temperature from the $L_{\rm X}$-kT relation above. The procedure is repeated until the estimated temperature converges. For clusters of galaxies the flux conversion factor has a median of 1.07×10^{-11} and varies by $\pm 16\%$ over the full range of column densities and redshifts sampled by the NEP clusters. For stars a Raymond-Smith plasma spectrum with a temperature of 10^7 K, a solar metallicity abundance, and no Galactic absorption were assumed, resulting in a conversion factor of 5.95×10^{-12}.

To correct for flux outside the detect cell a size correction for point sources has been applied by calculating the integral of the RASS point-spread function, or PSF (Boese 2000), at 1 keV within the circular detect aperture of $5'$ radius. The correction applied is 1.0369, which corresponds to the reciprocal of the integral of the PSF within the circle. For extended sources like galaxy clusters we adopted the β-model (Cavaliere & Fusco-Femiano 1976) surface brightness distribution $I(r) = I_o[1 + (r/r_c)^2]^{-(3\beta-0.5)}$, with a core radius, r_c, equal to 0.25 Mpc with $\beta = 2/3$. The β model surface brightness is convolved with the RASS PSF and integrated out to infinity.[5] Then this integral is divided by the integral within the $5'$ circle aperture to obtain the size correction. The median size correction for clusters is 1.33. At the median redshift of the NEP cluster sample ($z = 0.2$) the size correction varies by only $\pm 5\%$ for core radii between 0.2 and 0.3 Mpc.

K-corrected luminosities are computed for the extragalactic objects in the NEP survey using the redshift particular to each source. For clusters of galaxies the K-corrections were computed assuming again a Raymond-Smith plasma spectrum with a metallicity of 0.3 solar. The median K-correction for the NEP clusters is 0.95. For AGNs the adopted power-law spectrum with energy index -1 results in a K-correction equal to 1. Unabsorbed detect fluxes ($f_{\rm det}$) and total fluxes ($f_{\rm tot}$) in the *ROSAT* rest frame are reported in Table 3 (see § 5), together with K-corrected luminosities in the source rest frame (all in the *ROSAT* hard band 0.5–2.0 keV).

The selection function for the NEP sources is described in detail by Mullis (2001) and Henry et al. (2001), including the *ROSAT* NEP sky coverages for AGNs, clusters, and stars.

3. OPTICAL IDENTIFICATION PROCEDURE

A comprehensive program of optical follow-up observations to determine the nature of each of the X-ray sources in the NEP sample led to the identification of all but two NEP sources. There is evidence that at least one of the two unidentified sources is a blend and that both may be statistical fluctuations. Note, two spurious sources are expected in a sample of 445 objects (see § 2). The NEP is observable from mid-May until mid-August from Hawai'i. The optical identification program began in the summer of 1991, just a few months after the RASS was finished, and ended in the summer of 2000. We made most of the optical observations from Mauna Kea, where 126 nights were assigned of which 100 were clear. We spent 101 nights at the University of Hawai'i (UH) 2.2 m telescope, 17 nights at the Canada-France-Hawai'i (CFH) 3.6 m telescope, and eight nights at the Keck 10 m telescope. Additional observations were made at Mount Hopkins, where five nights at the Multiple Mirror Telescope (MMT) were assigned, of which two were clear and a clear night of 1.5 m telescope was also used. In total we used 132 nights of which 103 were clear (see Table 1).

The procedure used to identify an X-ray source is essentially that described in Stocke et al. (1991) for the EMSS survey. The process with the NEP survey is considerably easier since the positional uncertainty of the RASS is $15\farcs7$, about 15 times smaller in area than the *Einstein* IPC ($15\farcs7$ vs. $\sim 60''$). The EMSS had between one and eight objects in its error circle visible on the POSS plates and often had to use an X-ray to optical flux criterion to discriminate between more than one plausible counterpart in their large error circle. Whereas for 93% of NEP sources, there are ≤ 2 objects in the error circle visible in the DSS and it is very rare to have more than one plausible identification fall within the

[4] Luminosities in the *ROSAT* rest-frame are transformed in luminosities into the object's rest frame using the K-correction, in the 0.5–2.0 keV band, defined as $k_{0.5-2.0} = \left(\int_{0.5}^{2.0} f_E dE\right) > / \left(\int_{0.5(1+z)}^{2.0(1+z)} f_E dE\right)$, where f_E is the differential flux (flux per unit energy) as a function of energy and the integration limits are energy band edges in keV.

[5] The difference between integrating out to infinity and to 12 core radii is about 8%.

TABLE 1
OPTICAL FOLLOW-UP OBSERVATIONS

Telescope	Nights Assigned	Nights Clear
Mauna Kea:	126	100
UH 2.2 m	101	...
CFHT 3.6 m	17	...
Keck 10 m	8	...
Mount Hopkins:	6	3
MMT	5	2
1.5 m	1	1
Total	132	103

error circle. The 15″7 positional accuracy of the NEP survey has been computed by using the offset from the X-ray position within which 90% of the point sources (AGNs and stars) fall. Figure 1 shows an histogram of the angular offsets between the X-ray sources and their optical counterparts with the 15″7 offset indicated by the vertical dotted line. The basic procedure is to spectroscopically examine objects in close proximity on the sky to the X-ray source until a likely optical counterpart is located. The search begins with the object closest to the X-ray source position or with a blue stellar object if such a source is present in the positional error circle.

We started by inspecting finding charts of the 445 NEP sources prepared from the Automated Plate Machine (APM) object catalog (Hook et al. 1996). The APM scanned both colors of the Palomar Observatory Sky Survey photographic plates (POSS-I, Wilson 1952; California Institute of Technology 1954) providing a matched object catalog down to $m = 21.5$ in blue (O, 3200–4900 Å) and $m = 20$ in red (E, 6200–6800 Å). These passbands resemble the Johnson B and Kron-Cousins R except for the narrowness of the E passband. Magnitudes have an internal accuracy of 0.1 mag for objects brighter than 1 mag above the plate limit, and a typical external accuracy of 0.5 mag. The APM also classifies objects as either stellar, nonstellar, or a blend of multiple

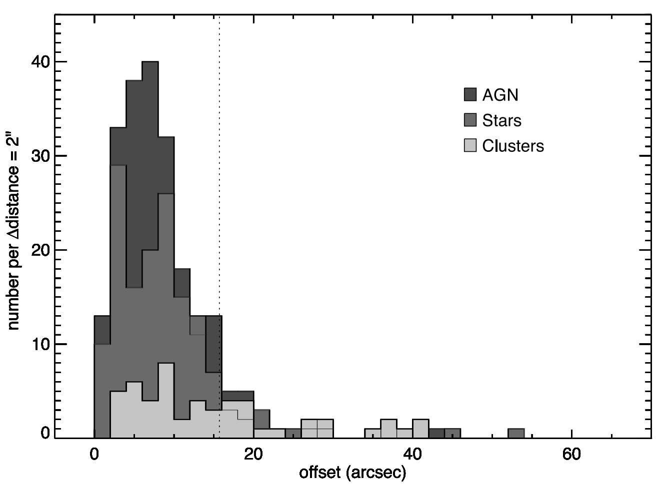

FIG. 1.—Angular position offsets between the NEP X-ray sources and their optical counterparts. AGNs are shown in dark gray, stars in medium gray, and galaxy clusters in light gray. The vertical line at 15″7 indicates the offset from the X-ray position within which 90% of the AGNs and stars fall (adapted from Fig. 3.5 of Mullis 2001).

sources. Overlays of optical and X-ray images of the NEP sources were also prepared using the second Palomar Observatory Sky Survey (POSS-II) and the RASS data in order to check the APM classifications, resolve the blends, and extend the magnitude limit. Digitized Sky Survey (DSS) images of the POSS-II red plates were obtained using the STScI *WWW* interface.[6] The full catalog of the finding charts and the overlaid X-ray contours will appear in a forthcoming paper (see also Appendix C in Mullis 2001). Through the inspection of the optical plus X-ray contour finders, and aided by the APM object catalog and by cross-correlations with SIMBAD and NED databases,[7] small percentages of X-ray sources were immediately identifiable with previously known X-ray emitters (5%) and very bright stars (~11%). The bright star identifications were only made where evidence for alternate counterpart was absent. During the inspection of the finders a preliminary target list was compiled for spectroscopic follow-up of the objects within the 90% confidence error circle of 15″7. Ten percent of the sources had zero visible sources, 55% had one, 28% had two, 5% had three, and 2% had four or more visible sources within the error circle. Extremely blue stellar objects ($O - E \leq 1.3$) were given priority as these sources are almost always AGNs. Fields with an overdensity of galaxies were flagged as potential cluster candidates as were fields that contain a few galaxies at the limits of the DSS finders.

The surface density of plausible X-ray counterparts and the positional uncertainties of the X-ray data are sufficiently low that only one plausible counterpart is likely to fall in the positional error circle. Hence, confusion levels are negligible in the NEP survey and can be quantified. We have computed the number of objects that may be found in the error circle by chance. Using the AGN optical surface densities from Boyle, Shanks, & Peterson (1988), a contamination rate of false-positive less than 1% at $B < 20.7$[8] is obtained, only one "random" AGN is expected out of 190 AGNs observed at $B < 20.7$. Using the Galactic model of Wainscoat et al. (1992) to estimate the number of plausible stellar counterparts randomly present in the survey, we proceeded as follows. Given the high certainty of the AGN identifications, we removed those sources leaving 228 NEP error circles that subtend 0.0136 deg^2 of the sky. At $B < 17.2$, 137 F-M stars are observed where 12 coincidences with F-M are expected. Thus, the false-positive rate for $B < 17.2$ is 9% (or 12/137).

Though detailed spectral classifications for the NEP stellar identifications was not attempted in all cases, it is possible to reliably confirm M dwarfs due to the distinctive TiO absorption bands in their spectra. Approximately 16% of the NEP X-ray sources identified with stars are M dwarfs, of which 20 have $B < 18.6$. Using the solid angle of all non-AGN NEP sources (0.0136 deg^2) and considering the source density of M stars down to $B < 18.6$, only one M star would fall into the error circle by random chance. Consequently, the false-positive rate for M dwarfs down to $B < 18.6$ is 5% (1/20), while the rate for the remaining F-K dwarfs is 6% down to $B < 16.3$ (seven coincidences expected against 114 observed). Hence, the random probability of a late-type

[6] http://archive.stsci.edu/dss.
[7] http://simbad.harvard.edu and http://nedwww.ipac.caltech.edu.
[8] We have approximated the B magnitudes using the O magnitudes from the APM.

dwarf falling in the NEP positional error circles is quite low, though not as low as for AGNs.

We refer the reader to Mullis (2001, see his chap. 4) for additional details on the optical identification procedure.

3.1. *Optical Imaging Observations*

A program of optical imaging was undertaken to observe those fields around the NEP sources that exhibited no objects in the X-ray error circle of the APM or DSS data. The distant cluster candidates were also observed. Images in two colors, *B* and *I* (Kron-Cousins) bands, were obtained at the UH 2.2 m to discriminate between AGNs (usually blue) and the cores of galaxy clusters, predominantly populated by red, early-type galaxies. We used the TEK 2048^2 CCD at the f/10 focus of the UH 2.2 m telescope, which gives a scale of 0.″22 pixel^{-1} and a field of view (FOV) of approximately 7.5×7.5 arcmin^2. The exposures were typically 10 minutes in both bands resulting in limiting magnitudes of $\sim$23 in *B* and $\sim$22 in *I*. Additional 30 minute exposures were obtained for sources that were eventually identified as distant clusters. Photometric calibration of the imaging data used the M92 standards (Christian et al. 1985; Heasley & Christian 1986).

3.2. *Spectroscopic Observations*

In parallel to imaging we acquired low-resolution spectra of objects starting with the one closest to the X-ray source position and then going out to larger offsets until the first plausible counterpart was found. Alternatively, if a blue stellar object was present in the positional error circle, the search began with that object and then proceeded to other objects if necessary. In either case, if there was evidence of an overdensity of faint objects close to the X-ray source in the imaging data, additional spectra were obtained to test for the presence of a galaxy cluster. Particular attention was given to assure that clusters were not missed due to close projections with bright stars or due to AGNs in the cluster environment. Most of the spectroscopy at the beginning was done using the UH 2.2 m Wide-Field Grism Spectrograph (WFGS), but we also used the Multi-Object-Spectrograph (MOS) on the CFHT 3.6 m, and the Low-Resolution Imaging Spectrograph (LRIS; Oke et al. 1995) on Keck.

At the UH 2.2 m telescope we used the 420 line mm^{-1} red grism and a 200 μm slit (1.8 arcsec^{-1}), which provided at the f/10 focus a pixel scale in spectroscopic mode of 3.6 Å pixel^{-1}, a spectral resolution of $\sim$19 Å FWHM, and a wavelength coverage of approximately 3800–9000 Å. In imaging mode the FOV is 4.75×4.75 arcmin^2 and the image scale is 0.″35 pixel^{-1}. Observations at the MMT were made with the MMT spectrograph using a 280 μm slit (1 arcsec^{-1}) with the 300 line mm^{-1} grating, which provides a dispersion of 1.96 Å pixel^{-1} and a spectral resolution of $\sim$6 Å FWHM (Foltz & Smith 1994). Observations at the FLWO (F. L. Whipple Observatory) 1.5 m telescope were made with the photon counting Reticon system (Latham 1982) and 3″ slit, which also provides a resolution of $\sim$6 Å FWHM.

The instrument setups for other telescopes, although different, provided similar performance. The UH 2.2 m telescope was used to observe both stars and AGNs, but also to acquire long-slit spectra of relatively bright cluster galaxies. Multiobject spectra were subsequently taken with CFH and Keck telescopes for the fields around X-ray sources that showed overdensities of faint galaxies. This multiobject spectroscopy approach was a departure from the Stocke et al. (1991) procedure and provides more confidence in any cluster identifications since many concordant redshifts could be obtained. In total over 1000 objects were observed spectroscopically. Calibration data were based on spectrophotometric standard stars of Oke & Gunn (1983) and Massey et al. (1988).

The optical data were analyzed using standard IRAF[9] reduction packages and IDL[10] routines. A quick reduction and interpretation of long-slit spectra were normally completed in "real-time" at the telescope in order to decide if further spectra were required to make a reliable identification of a particular X-ray source. Nonetheless, all data were subsequently reduced off-line using standard procedures. Spectra were classified according to the presence or absence of various absorption and emission lines and the shape of the continuum emission. Once features have been identified, the redshift of a source was measured based on the offset of the features from their rest-frame wavelengths (typical redshift uncertainty $\delta z \lesssim 0.001$). Commonly observed absorption lines included the Ca II H and K doublet, the 4000 Å break, the *G* band, Mg I *b*, Na I *d*, and Hα. Often present emission lines included Mg II, [O II] λ3727, Hβ, [O III] λ4959, [O III] λ5007, and sometimes Hα.

4. IDENTIFICATION CONTENT

For the classification of the optical counterparts to the NEP X-ray sources we have followed the pioneering work of Stocke et al. (1991) for the EMSS survey. Table 2 presents a summary of the identifications of the NEP X-ray sources. Sixty-five percent of the extragalactic counterparts and nearly half (49.4%) of all sources are AGNs, whose spectra normally are characterized by the presence of emission lines and have a blue relatively featureless continuum. The classification with AGNs has been done on the basis of equivalent width of the emission lines (W_λ) and broadness (FWHM) of the permitted emission lines. AGNs showing a QSO like spectrum with a $W_\lambda \geq 5$ Å, and broad permitted emission lines (FWHM $\geq$ 2000 km s^{-1}), have been classified as AGN type 1 ("AGN1" in Table 3). This class includes QSO objects and Seyfert 1 galaxies. Examples of this kind of spectra are shown in Figures 2, 3, and 4. Type 2 AGNs ("AGN2" in Table 3) have similar permitted and forbidden emission lines, both narrow and with a FWHM $<$ 2000 km

[9] http://iraf.noao.edu.
[10] http://www.rsinc.com.

TABLE 2
SUMMARY OF THE *ROSAT* NEP X-RAY SOURCE IDENTIFICATIONS

Type	Number	Percentage[a]
AGN	219	49.4
Star	152	34.3
Galaxy cluster	62	14.0
BL Lac	8	1.8
Galaxy	1	0.2
Planetary nebula	1	0.2
No identification	2	0.4

[a] Out of 443 for identifications, out of 445 for nonidentifications.

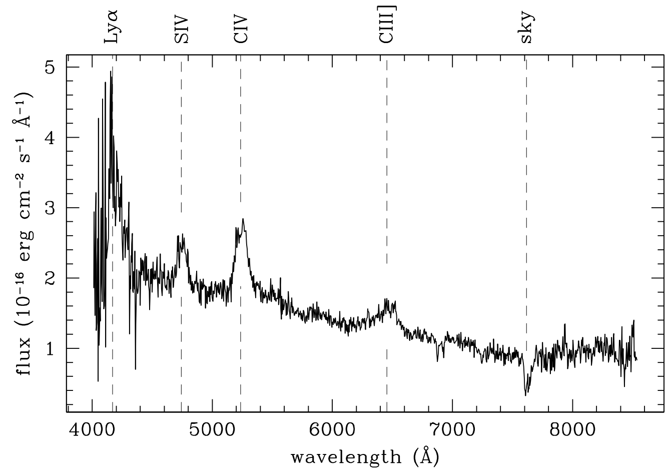

FIG. 2.—RX J1747.1+6813: AGN1 at $z = 2.392 \pm 0.002$ ($\alpha_{2000} = 17^h47^m12^s.7$, $\delta_{2000} = +68°13'26''$). Long-slit spectrum of a distant QSO obtained with the UH 2.2 m telescope on 1998 June 19. The total integration time was 20 minutes. The dashed lines indicate the positions of the emission lines at the AGN1 redshift. Wavelengths of atmospheric absorption bands are also indicated.

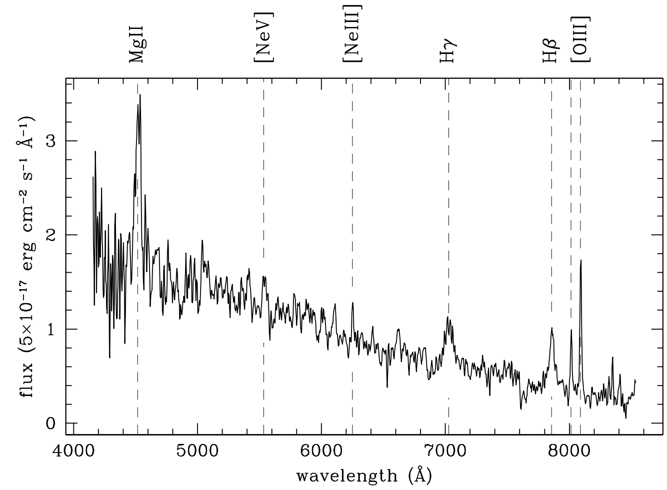

FIG. 4.—RX J1813.6+6731: AGN1 at $z = 0.6168 \pm 0.0004$ ($\alpha_{2000} = 18^h13^m43^s.0$, $\delta_{2000} = +67°32'23''$). Long-slit spectrum of a QSO obtained with the U 2.2 m telescope on 1990 June 7. The total integration time was 30 minutes. The dashed lines indicate the positions of the emission lines at the AGN1 redshift. Wavelengths of atmospheric absorption bands are also indicated.

s^{-1}, mostly much narrower than the limit of 2000 km s^{-1}. Type 2 AGNs include Seyfert 2 and star-forming galaxies. Examples of AGN2 spectra are shown in Figures 5 and 6. Some of the cluster galaxies in the NEP catalog show spectral similarities to AGN2. Even in these cases the X-ray source is identified as a cluster. See Figure 7 for the spectrum of a Sy2 galaxy at $z = 0.3665$ in a cluster at $z = 0.3652$. There are four spirals with lines having FWHM $<$ 2000 km s^{-1}; they have been classified as AGN2 and are indicated in Table 3. This number is, however, a lower limit since only for the nearby objects it is possible to make a morphological classification. The redshift distribution for the AGNs in bins of $\Delta z = 0.1$ is shown in Figure 8 (*dark gray*). The median and highest redshifts for AGNs are $z = 0.4$ and $z = 3.889$ (RX J1746.2+6227), respectively.

The second most common identification class is Galactic stars at 34.3%. Stellar counterparts to X-ray sources at the Galactic latitude of the NEP are usually late-type (F-M) stars whose spectra display hydrogen, metallic, and molecular absorption features. One planetary nebula (NGC 6543) was also detected as an X-ray source (RX J1758.5+6637; Kreysing et al. 1992).

Clusters and groups of galaxies comprise 14.0% of the sources. The identification of an X-ray source as a cluster of galaxies usually requires the absence of emission lines identifying AGNs, the absence of a nonthermal continuum identifying a BL Lac object, coupled with a centrally concentrated galaxy overdensity either from the POSS or from deep optical CCD images taken for more distant clusters, and at least two concordant redshifts. Multiobject

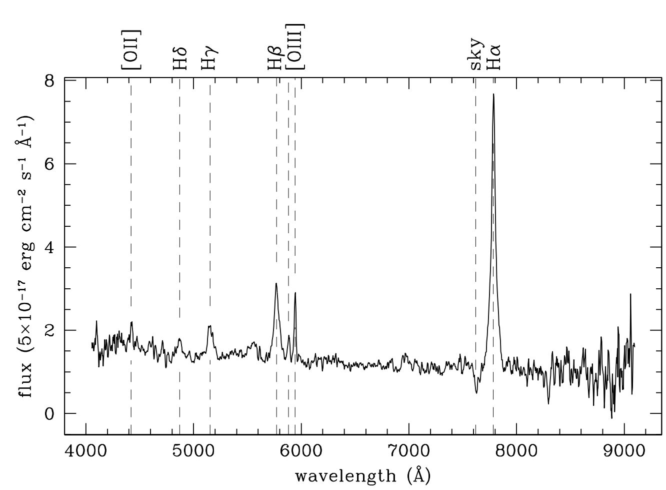

FIG. 3.—RX J1758.0+6851: AGN1 at $z = 0.1876 \pm 0.0005$ ($\alpha_{2000} = 17^h58^m03^s.7$, $\delta_{2000} = +68°51'51''$). Long-slit spectrum of a Sy1 galaxy obtained with the UH 2.2 m telescope on 1994 June 5. The total integration time was 30 minutes. The dashed lines indicate the positions of the emission lines at the AGN1 redshift. Wavelengths of atmospheric absorption bands are also indicated.

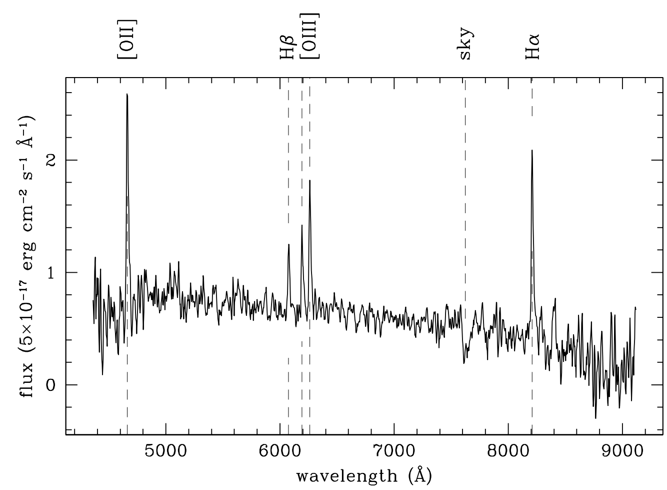

FIG. 5.—RX J1750.2+6415: AGN2 at $z = 0.2504 \pm 0.0003$ ($\alpha_{2000} = 17^h50^m15^s.1$, $\delta_{2000} = +64°14'56''$). Long-slit spectrum of a Sy2 galaxy obtained with the UH 2.2 m telescope on 1998 July 31. The total integration time was 20 minutes. The dashed lines indicate the positions of the emission lines at the AGN2 redshift. Wavelengths of atmospheric absorption bands are also indicated.

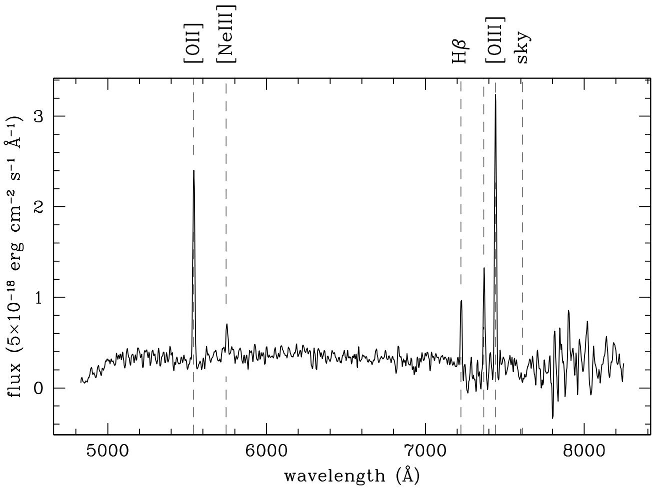

FIG. 6.—RX J1757.9+6609: AGN2 at $z = 0.4865 \pm 0.0002$ ($\alpha_{2000} = 17^h57^m56\overset{s}{.}5$, $\delta_{2000} = +66°09'20''$). Long-slit spectrum of a Sy2 galaxy obtained with Keck II LRIS on 1998 July 16. The total integration time was 30 minutes. The dashed lines indicate the positions of the emission lines at the AGN2 redshift. Wavelengths of atmospheric absorption bands are also indicated.

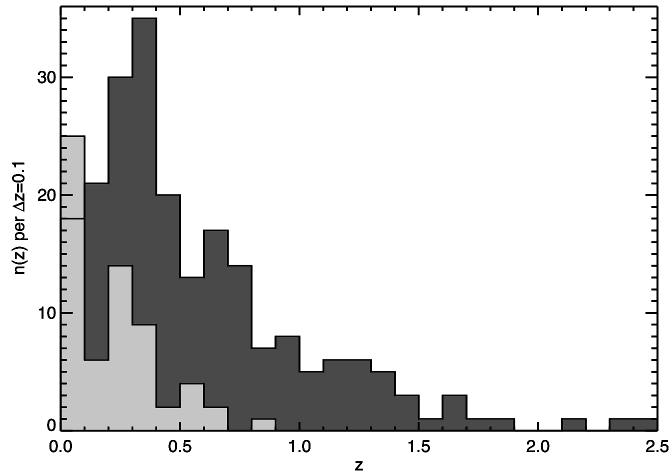

FIG. 8.—Redshift distributions of NEP AGNs (*dark gray*) and clusters of galaxies (*light gray*) in bins of $\Delta z = 0.1$. To preserve the readibility of this plot the highest redshift AGN1 (RX J1746.2+6227, $z = 3.889$, $L_X = 4.65 \times 10^{46}$ ergs s^{-1}) is not shown.

spectroscopy was performed for several fields around X-ray sources that showed overdensities of faint galaxies. Many of the sources proved to be distant clusters ($z \geq 0.3$). The optical spectrum of a galaxy in the highest-z cluster of the NEP survey (RX J1821.6+6827, $z = 0.811$) is shown in Figure 9. Two more spectra of galaxies in clusters (RX J1745.2+6556 at $z = 0.608$ and RX J1817.7+6824 at $z = 0.282$) are given in Figures 10 and 11, respectively. The median and highest redshift for clusters of galaxies are, respectively, 0.205 and 0.811. Their redshift distribution in bins of $\Delta z = 0.1$ is shown in Figure 8 (*light gray*).

A featureless, blue continuum without any line emission or significant 4000 Å break suggests a BL Lacertae type object. The optical spectrum is characterized by $W_\lambda \leq 5$ Å, either for emission or absorption lines, and a Ca II H and K "break" (when present) less than 25%. The very weak equivalent width limit for any emission lines present separates the BL Lac objects from the weak-line AGNs. The limit of 25% of the flux depression discontinuity blueward across the Ca II break is significantly less than the 50% contrast possessed by a normal elliptical galaxy. This limit is imposed to ensure the presence of a substantial nonthermal continuum and thus discriminate BL Lac objects from normal galaxies. See extensive discussion of this point in § 3.1.2 of Stocke et al. (1991). There are eight BL Lacertae objects in the NEP survey (1.8%), of which four (RX J1727.0+6926, RX J1742.7+6852, RX J1759.8+7037, and RX J1803.9+6548) are new discoveries.

One source is identified as individual galaxy (GAL in Table 3). This source is associated with an individual,

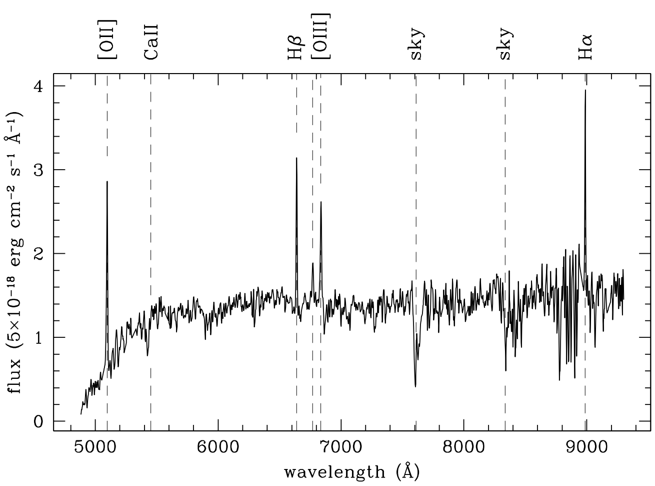

FIG. 7.—RX J1758.9+6520: cluster of galaxies at $z = 0.3652 \pm 0.0008$. Long-slit spectrum of a cluster member, galaxy C ($\alpha_{2000} = 17^h58^m53\overset{s}{.}8$, $\delta_{2000} = +65°21'02''$, $z = 0.3665 \pm 0.0008$), which shows AGN2 spectral features. The spectrum was obtained with Keck II LRIS on 1998 July 16. The total integration time was 30 minutes. The dashed lines indicate the positions of emission lines and of the stellar absorption features at the AGN2 redshift. Wavelengths of atmospheric absorption bands are also indicated.

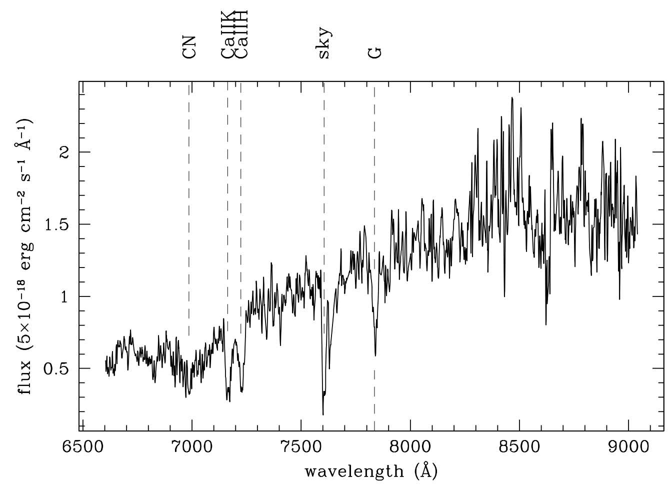

FIG. 9.—RX J1821.6+6827: cluster of galaxies at $z = 0.8108 \pm 0.0012$. Spectrum of the cluster galaxy 116 ($\alpha_{2000} = 18^h21^m26\overset{s}{.}3$, $\delta_{2000} = +68°29'28''$, $z = 0.8202 \pm 0.0001$) obtained with Keck I LRIS in multislit mode on 2001 June 23. The total integration time was 2.25 hr. The dashed lines indicate the positions of stellar absorption features at the cluster redshift. Wavelengths of atmospheric absorption bands are also indicated.

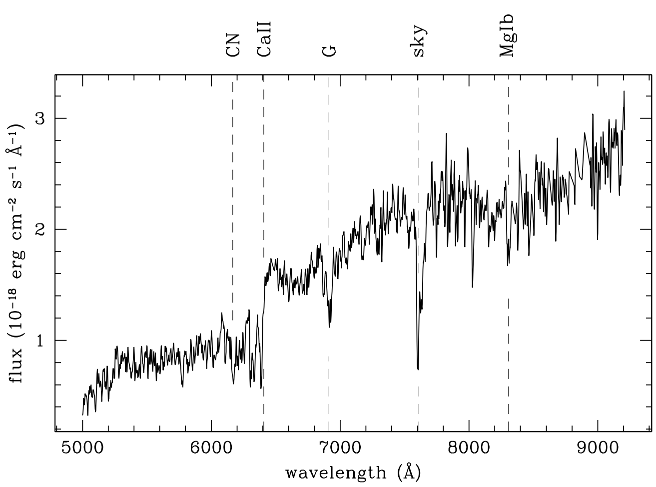

FIG. 10.—RX J1745.2+6556: cluster of galaxies at $z = 0.608 \pm 0.0005$. Long-slit spectrum of the cluster galaxy B ($\alpha_{2000} = 17^h45^m18^s.2$, $\delta_{2000} = +65°55'42''$, $z = 0.6077 \pm 0.0009$) obtained with Keck II LRIS on 1998 June 26. The total integration time was 30 minutes. The dashed lines indicate the positions of stellar absorption features at the cluster member redshift. Wavelengths of atmospheric absorption bands are also indicated.

non-AGN galaxy (RX J1806.4+7028, $z = 0.0971$). However, this apparently isolated galaxy has an X-ray luminosity commensurate with that of a high-luminosity galaxy group or low-luminosity galaxy cluster ($\sim 2 \times 10^{43}$ ergs s^{-1}, 0.5–2.0 keV). As first pointed out by Mullis (2001), this is likely an example of an X-ray overluminous elliptical galaxy (OLEG; Vikhlinin et al. 1999) or a "fossil group" (Ponman et al. 1994), postulated to be the result of galaxy merging within a group.

There are a few cases in which the identification is ambiguous. For instance, in the field of one source, identified with an AGN1 (RX J1720.8+6210) at $z = 0.7313$, there are two galaxies at the same redshift as the AGN1 and closer to the X-ray position. In this case the presence of a distant cluster with similar redshift is not excluded. Other cases include sources identified with clusters (i.e., RX J1745.2+6556 at $z = 0.608$; see Figure 10 for the spectrum of a member galaxy at $z = 0.6077$) where an AGN at a different redshift ($z = 0.2904$) from the cluster redshift, is present in the field and could contribute to the X-ray emission of the source. There are also two examples of X-ray sources identified as cluster plus AGN. Namely, RX J1758.9+6520 ($z = 0.3652$) and RX J1806.1+6813 ($z = 0.303$), are two sources identified as clusters of galaxies even if the contribution to the X-ray emission of an AGN1 (in each case at the same redshift as the cluster) is not excluded. Other cases include X-ray sources with two AGNs present in their error circles. Only high-resolution and high-sensitivity X-ray observations would allow us to identify the X-ray source unambiguously. The number of these ambiguous identifications is very low (~1%). They are all reported in § 6.

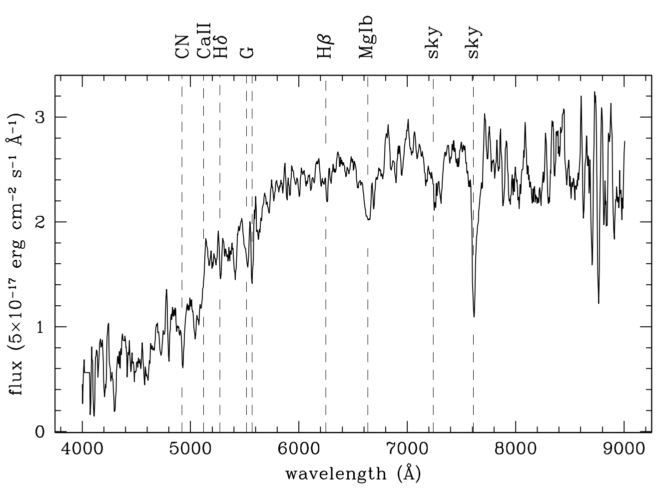

FIG. 11.—RX J1817.7+6824: cluster of galaxies at $z = 0.282 \pm 0.002$. Long-slit spectrum of the cluster cD galaxy A ($\alpha_{2000} = 18^h17^m44^s.7$, $\delta_{2000} = +68°24'24''$, $z = 0.282 \pm 0.002$) obtained with the UH 2.2 m on 1994 August 4. The total integration time was 30 minutes. The dashed lines indicate the positions of stellar absorption features at the cluster member redshift. Wavelengths of atmospheric absorption bands are also indicated.

Given the higher angular resolution of the *ROSAT* PSPC (~25″) compared with the *Einstein* IPC (~1′), there was no need to require a variety of optical and radio observations in order to conclusively identify the class of the optical counterpart to the NEP sources with confidence. However, both space-based and ground-based surveys of the NEP region have been performed, and the available source catalogs produced by those surveys have been scrutinized by us. We mention here the surveys of the NEP region from space completed by *IRAS* (Hacking & Houck 1987), *ISO* (Stickel et al. 1998; Aussel et al. 2000), and *COBE* (Bennet et al. 1996). From the ground, surveys were performed in radio by Kollgaard et al. (1994), Brinkmann et al. (1999), Rengelink et al. (1997), Loiseau et al. (1988), and Elvis et al. (1994), and in optical/IR by Gaidos, Magnier, & Schechter (1993) and Kümmel & Wagner (2000).

The distribution in the sky of the 445 NEP X-ray sources and their optical identification already appeared in the literature and are shown in Figure 4.12 of Mullis (2001) and in Figure 3 of Henry et al. (2001).

5. THE CATALOG

The 445 sources that form the *ROSAT* NEP source catalog are presented in Table 3. The columns contain the following information:

Column (1).—Source name formed by the acronym RX J (*ROSAT* X-ray source, Julian 2000 position), and the X-ray centroid position.

Column (2).—Internal source identification number, which runs between 10 and 6570.

Column (3).—Right ascension of the X-ray centroid (J2000, HH MM SS.S).

Column (4).—Declination of the X-ray centroid (J2000, +DD MM SS).

Column (5).—Right ascension of the optical object associated with the X-ray source (J2000, HH MM SS.S).

Column (6).—Declination of the optical object associated with the X-ray source (J2000, +DD MM SS).

Column (7).—Signal-to-noise on the detected source count rate determined as net source count rate over 1 σ uncertainty on the count rate.

Column (8).—Detect unabsorbed flux in the 0.5–2.0 keV band ($f_{X,\rm det}$, 10^{-14} ergs cm^{-2} s^{-1}). The detect flux is measured in the photometry circular aperture (5′ radius). To determine the fluxes for the different classes of astronomical objects we have converted from count rate to unabsorbed

TABLE 3

ROSAT NEP Source Catalog

Object (1)	NEP Scan No. (2)	α_X (J2000) (3)	δ_X (J2000) (4)	α_{opt} (J2000) (5)	δ_{opt} (J2000) (6)	S/N (7)	$f_{X,det}$ (10^{-14}) (8)	$f_{X,tot}$ (10^{-14}) (9)	L_X (10^{44}) (10)	z (11)	ID (12)	Notes (13)
RX J1715.4+6239	1239	17 15 25.3	+62 39 34	17 15 25.7	+62 39 27	4.6	18.90	19.60	8.09	0.8500	AGN2	
RX J1715.6+6856	1240	17 15 41.4	+68 56 31	17 15 41.7	+68 56 43	5.3	8.81	9.14	...	...	Star	
RX J1715.6+6231	1241	17 15 41.6	+62 31 33	17 15 42.3	+62 31 27	4.4	10.12	10.49	...	...	Star	
RX J1716.2+6836	1270	17 16 14.4	+68 36 36	17 16 13.8	+68 36 38	20.2	138.48	143.59	48.70	0.7770	AGN1	n
RX J1716.6+6410	1271	17 16 39.7	+64 10 35	17 16 42.3	+64 10 41	6.5	23.88	30.91	0.86	0.2507	CL	sc = 1.295
RX J1717.1+6401	1272	17 17 08.1	+64 01 46	17 17 07.1	+64 01 45	9.3	44.81	46.47	0.38	0.1334	AGN1	
RX J1717.5+6559	1300	17 17 35.6	+65 59 35	17 17 37.9	+65 59 39	9.0	53.45	55.42	2.33	0.2936	AGN1	
RX J1717.7+6431	1320	17 17 44.4	+64 31 45	17 17 47.4	+64 31 41	5.7	19.10	19.81	0.01	0.0337	AGN2	n, spiral
RX J1717.9+7038	1330	17 17 57.0	+70 38 15	17 17 56.6	+70 38 16	10.2	58.36	60.52	0.85	0.1738	AGN2	
RX J1718.0+6727	1340	17 18 05.5	+67 27 11	17 18 05.9	+67 27 00	7.4	24.32	25.21	4.05	0.5506	AGN1	
RX J1718.3+6754	1350	17 18 20.4	+67 54 32	17 18 19.6	+67 54 17	4.7	5.60	5.80	...	...	Star	
RX J1719.0+6852	1400	17 19 01.2	+68 52 33	17 19 00.9	+68 52 32	7.8	16.25	16.85	...	...	Star M	
RX J1719.0+6929	1410	17 19 03.6	+69 29 33	17 19 03.5	+69 29 39	4.8	15.35	15.92	0.61	0.2816	AGN1	
RX J1719.4+6522	1420	17 19 28.8	+65 22 27	17 19 28.8	+65 22 29	10.6	24.65	25.55	...	...	Star	
RX J1719.8+6457	1440	17 19 52.7	+64 57 48			4.4	7.47	7.75	...	...		n
RX J1720.0+6206	1441	17 20 05.0	+62 06 20	17 20 05.6	+62 06 22	5.7	18.99	19.69	...	...	Star	
RX J1720.1+6833	1450	17 20 07.8	+68 33 37	17 20 06.6	+68 33 50	6.5	20.42	21.17	3.25	0.5392	AGN1	
RX J1720.4+6703	1470	17 20 27.0	+67 03 45	17 20 26.7	+67 03 37	5.4	9.70	10.06	...	...	Star	
RX J1720.8+6210	1471	17 20 48.8	+62 10 13	17 20 42.3	+62 10 10	4.9	27.78	28.81	8.56	0.7313	AGN1	n
RX J1721.0+6711	1490	17 21 03.1	+67 11 54	17 21 02.3	+67 11 57	4.7	11.63	12.06	3.83	0.7538	AGN1	
RX J1721.1+6947	1500	17 21 10.7	+69 47 58	17 21 10.9	+69 48 02	4.6	6.55	6.79	...	...	Star F8	HD 158063
RX J1721.4+6733	1510	17 21 24.6	+67 33 14	17 21 24.9	+67 33 11	4.9	9.42	16.19	0.05	0.0861	CL	sc = 1.719
RX J1721.7+6200	1511	17 21 42.4	+62 00 36	17 21 42.5	+62 00 32	4.1	8.99	9.32	...	...	Star	
RX J1723.1+6826	1540	17 23 10.4	+68 26 54	17 23 09.9	+68 26 56	4.3	9.83	10.20	5.74	0.9782	AGN1	n
RX J1723.3+6333	1541	17 23 18.6	+63 33 34	17 23 17.9	+63 33 26	4.3	9.05	9.38	...	...	Star M	
RX J1724.0+6940	1580	17 24 00.1	+69 40 26	17 24 00.4	+69 40 30	10.9	28.45	29.50	...	...	Star	
RX J1724.1+7000	1590	17 24 11.6	+70 00 27	17 24 02.3	+69 58 01	4.2	11.11	32.42	0.02	0.0386	CL	sc = 2.919, n
RX J1724.2+6956	1591	17 24 16.0	+69 56 44	17 24 07.4	+69 54 58	4.2	11.98	34.96	0.02	0.0386	CL	sc = 2.919
RX J1724.4+6412	1600	17 24 27.0	+64 12 24	17 24 26.8	+64 12 23	5.1	9.94	10.31	...	...	Star	
RX J1724.6+6440	1601	17 24 39.1	+64 40 54	17 24 38.8	+64 40 51	5.0	7.68	7.96	...	...	Star	
RX J1724.7+6716	1630	17 24 47.3	+67 16 09	17 24 45.7	+67 16 13	4.4	7.70	9.95	0.29	0.2540	CL	sc = 1.292
RX J1724.9+6636	1640	17 24 55.5	+66 36 59	17 24 56.1	+66 36 50	4.0	12.38	12.84	3.25	0.6792	AGN1	
RX J1726.5+6714	1670	17 26 30.7	+67 14 12	17 26 28.6	+67 14 15	5.4	12.78	13.25	0.89	0.3659	AGN1	
RX J1726.7+6643	1680	17 26 43.9	+66 43 30	17 26 45.0	+66 43 19	9.1	46.78	48.51	3.33	0.3705	AGN1	
RX J1726.7+6937	1690	17 26 47.1	+69 37 43	17 26 45.4	+69 37 53	4.7	7.56	7.84	...	...	Star	
RX J1727.0+6926	1700	17 27 04.8	+69 26 58	17 27 04.5	+69 26 48	4.4	13.09	13.58	...	...	BL	n
RX J1727.2+6322	1710	17 27 12.0	+63 22 44	17 27 11.7	+63 22 41	11.7	91.06	94.42	2.10	0.2169	AGN1	
RX J1727.4+7035	1730	17 27 25.8	+70 35 37	17 27 33.6	+70 35 47	7.6	39.74	50.20	2.03	0.3059	CL	sc = 1.263
RX J1727.8+6748	1740	17 27 49.5	+67 48 43	17 27 45.5	+67 48 43	6.8	17.02	17.64	2.25	0.4950	AGN1	n
RX J1727.9+6210	1741	17 27 56.9	+62 10 54	17 27 56.6	+62 10 54	4.2	7.74	8.02	...	...	Star	
RX J1728.5+6732	1770	17 28 35.4	+67 32 33	17 28 34.6	+67 32 24	4.4	8.67	8.99	2.06	0.6493	AGN1	
RX J1728.6+7041	1780	17 28 39.5	+70 41 05	17 28 38.2	+70 41 03	5.5	23.42	28.26	3.65	0.5509	CL	sc = 1.207
RX J1729.0+6529	1781	17 29 01.2	+65 29 52	17 29 00.2	+65 29 52	5.2	7.14	7.41	...	...	Star	
RX J1729.2+7032	1782	17 29 12.0	+70 32 57	17 29 11.8	+70 32 55	4.4	16.54	17.15	2.62	0.5378	AGN1	
RX J1729.6+6847	1800	17 29 41.9	+68 47 41	17 29 39.4	+68 47 38	5.3	6.61	6.85	...	...	Star G	HD 159539
RX J1729.7+6737	1810	17 29 46.5	+67 37 54	17 29 46.1	+67 38 13	5.2	6.55	6.79	...	...	Star M	

TABLE 3—*Continued*

Object (1)	NEP Scan No. (2)	α_X (J2000) (3)	δ_X (J2000) (4)	α_{opt} (J2000) (5)	δ_{opt} (J2000) (6)	S/N (7)	$f_{X, det}$ (10^{-14}) (8)	$f_{X, tot}$ (10^{-14}) (9)	L_X (10^{44}) (10)	z (11)	ID (12)	Notes (13)
RX J1730.1+6247	1820	17 30 07.9	+62 47 44	17 30 08.4	+62 47 55	10.5	35.54	36.85	...	...	Star	
RX J1730.3+6955	1840	17 30 20.5	+69 55 23	17 30 19.9	+69 55 27	10.1	25.90	26.85	...	...	Star	
RX J1732.0+6926	1910	17 32 05.5	+69 26 22	17 32 04.5	+69 26 39	5.7	17.61	18.26	2.43	0.5043	AGN1	
RX J1732.5+7031	1920	17 32 31.3	+70 31 37	17 32 31.0	+70 31 31	8.1	42.89	44.47	0.94	0.2114	AGN1	n
RX J1732.9+6533	1930	17 32 54.5	+65 33 24	17 32 53.9	+65 33 25	10.1	40.92	42.43	17.79	0.8560	AGN1	n
RX J1733.2+6712	1960	17 33 16.8	+67 12 28	17 33 16.9	+67 12 08	9.8	16.25	16.85	...	...	Star F2	HD 160198
RX J1734.5+6755	1980	17 34 30.3	+67 55 05	17 34 27.8	+67 55 04	4.7	9.88	10.24	0.27	0.2341	AGN1	
RX J1735.0+6405	2020	17 35 04.9	+64 05 57	17 35 04.6	+64 06 05	12.4	75.00	108.81	0.94	0.1411	CL	sc = 1.451, A 2276
RX J1736.0+6559	2040	17 36 00.0	+65 59 00	17 36 01.9	+65 58 54	4.5	11.03	11.43	1.10	0.4341	AGN1	
RX J1736.2+6502	2050	17 36 14.6	+65 02 29	17 36 14.1	+65 02 27	18.2	60.84	63.08	...	...	Star	
RX J1736.3+6802	2051	17 36 23.4	+68 02 06	17 36 09.3	+68 05 32	13.2	54.72	246.42	0.07	0.0258	CL	sc = 4.503, n
RX J1736.4+6820	2100	17 36 27.1	+68 20 30	17 36 26.6	+68 20 37	15.5	36.91	38.27	...	...	Star	n
RX J1736.9+6845	2130	17 36 57.6	+68 45 21	17 36 57.0	+68 45 12	45.2	277.11	287.33	...	...	Star F5 V	n, SAO 17576
RX J1737.0+6601	2131	17 37 05.5	+66 01 05	17 37 07.8	+66 01 02	6.7	16.56	17.17	1.10	0.3580	AGN2	
RX J1738.0+6653	2132	17 38 01.3	+66 53 36	17 38 02.3	+66 53 47	5.4	6.43	6.67	...	...	Star	
RX J1738.0+6314	2150	17 38 01.5	+63 14 21	17 38 01.3	+63 14 22	4.1	6.91	7.16	...	...	Star	
RX J1738.0+6210	2160	17 38 02.6	+62 10 42	17 38 03.8	+62 10 54	4.8	13.19	13.68	18.14	1.4402	AGN1	
RX J1738.0+6509	2170	17 38 04.8	+65 09 33	17 38 04.4	+65 09 32	9.5	16.91	17.53	...	...	Star M	
RX J1738.4+6417	2180	17 38 24.0	+64 17 59	17 38 24.5	+64 17 56	5.5	14.48	15.01	5.36	0.7955	AGN1	
RX J1738.7+7037	2200	17 38 42.0	+70 37 05	17 38 42.0	+70 37 16	7.8	34.24	35.50	0.32	0.1399	AGN1	
RX J1739.2+7020	2210	17 39 16.2	+70 20 09	17 39 16.1	+70 20 09	5.8	11.49	11.91	...	...	Star F8	SAO 8868
RX J1739.3+6614	2211	17 39 21.5	+66 14 41	17 39 25.8	+66 14 31	4.1	9.11	9.45	10.78	1.3460	AGN1	
RX J1739.7+6710	2230	17 39 44.6	+67 10 52	17 39 44.7	+67 10 43	12.6	41.24	42.77	0.27	0.1180	AGN1	n
RX J1739.9+6500	2250	17 39 55.8	+65 00 07	17 39 56.1	+65 00 04	10.8	21.31	22.10	...	...	Star K0	
RX J1739.9+7005	2240	17 39 56.0	+70 05 52	17 39 54.2	+70 05 57	6.0	20.02	20.76	2.96	0.5209	AGN1	
RX J1740.7+6255	2290	17 40 44.0	+62 55 08	17 40 44.6	+62 55 12	5.5	9.23	9.57	...	...	Star	
RX J1741.2+6507	2300	17 41 14.4	+65 07 43	17 41 15.7	+65 07 42	6.3	16.02	16.61	5.16	0.7466	AGN1	n
RX J1741.7+6335	2320	17 41 46.0	+63 35 13	17 41 45.6	+63 35 22	6.5	18.64	19.33	83.72	2.4420	AGN1	
RX J1742.2+6639	2340	17 42 12.5	+66 39 49	17 42 13.8	+66 39 34	6.6	15.44	16.01	16.11	1.2720	AGN1	
RX J1742.2+6936	2341	17 42 15.1	+69 36 29	17 42 16.6	+69 36 21	4.3	11.71	12.14	7.94	1.0470	AGN1	
RX J1742.2+6351	2350	17 42 17.9	+63 51 09	17 42 18.4	+63 51 15	10.2	43.42	45.02	3.68	0.4019	AGN1	
RX J1742.4+6907	2360	17 42 26.9	+69 07 55	17 42 26.5	+69 07 58	5.2	6.25	6.48	...	...	Star G0	HD 161919
RX J1742.5+6709	2370	17 42 34.2	+67 09 36	17 42 33.8	+67 09 23	7.5	7.56	7.84	...	...	Star	
RX J1742.7+6800	2371	17 42 42.0	+68 00 11	17 42 43.5	+68 00 16	5.2	9.98	10.35	0.03	0.0858	AGN1	
RX J1742.7+6852	2380	17 42 43.4	+68 52 46	17 42 41.5	+68 52 53	6.0	15.18	15.75	...	...	BL	
RX J1742.7+6735	2381	17 42 46.8	+67 35 53	17 42 31.8	+67 35 33	10.1	29.18	79.17	0.06	0.0420	CL	sc = 2.713
RX J1743.0+6606	2400	17 43 02.3	+66 06 42	17 43 01.6	+66 06 46	15.0	27.74	28.76	...	...	Star G5	
RX J1743.3+6440	2410	17 43 23.3	+64 40 18	17 43 11.9	+64 39 47	8.7	28.74	39.43	0.56	0.1790	CL	sc = 1.372
RX J1743.4+6341	2420	17 43 28.1	+63 41 39	17 43 30.4	+63 41 41	10.5	40.23	50.49	2.33	0.3270	CL	sc = 1.255, n, A 2280
RX J1743.7+6829	2450	17 43 43.5	+68 29 26	17 43 42.9	+68 29 25	4.4	7.95	8.24	0.50	0.3504	AGN1	
RX J1743.8+6657	2460	17 43 49.2	+66 57 23	17 43 49.3	+66 57 08	4.2	6.58	6.82	0.85	0.4900	AGN1	
RX J1743.8+7031	2470	17 43 52.1	+70 31 37	17 43 51.7	+70 31 39	4.2	4.94	5.12	...	...	Star	
RX J1744.0+7015	2480	17 44 02.4	+70 15 27	17 44 00.6	+70 15 27	7.5	12.56	13.02	...	...	Star	
RX J1744.2+6534	2490	17 44 14.2	+65 34 54	17 44 14.5	+65 34 53	18.1	63.26	65.60	2.05	0.2550	AGN1	
RX J1744.5+6316	2510	17 44 31.9	+63 16 19	17 44 32.3	+63 16 33	5.0	6.91	7.16	...	...	Star	
RX J1744.9+6536	2550	17 44 55.0	+65 36 00	17 44 54.5	+65 36 02	5.1	7.10	7.36	0.46	0.3533	AGN1	
RX J1745.2+6609	2551	17 45 13.0	+66 09 38	17 45 12.1	+66 09 41	5.2	3.69	3.83	...	...	Star M	

TABLE 3—*Continued*

Object (1)	NEP Scan No. (2)	α_X (J2000) (3)	δ_X (J2000) (4)	α_{opt} (J2000) (5)	δ_{opt} (J2000) (6)	S/N (7)	$f_{X, det}$ (10^{-14}) (8)	$f_{X, tot}$ (10^{-14}) (9)	L_X (10^{44}) (10)	z (11)	ID (12)	Notes (13)
RX J1745.2+6556	2560	17 45 16.2	+65 56 17	17 45 18.2	+65 55 42	4.6	5.90	7.09	1.19	0.6080	CL	sc = 1.201, n
RX J1745.4+6918	2580	17 45 25.9	+69 18 19	17 45 24.5	+69 18 21	11.8	23.22	24.07	...	...	Star	
RX J1745.6+6543	2600	17 45 40.8	+65 43 46	17 45 41.3	+65 43 49	5.2	3.99	4.14	...	...	Star	
RX J1745.7+6748	2610	17 45 42.6	+67 48 15	17 45 42.4	+67 48 14	4.5	6.99	7.25	0.63	0.4143	AGN2	
RX J1745.9+6451	2650	17 45 55.2	+64 51 18	17 45 55.5	+64 51 25	8.8	24.40	25.30	0.38	0.1790	AGN1	
RX J1746.0+6727	2670	17 46 03.0	+67 27 09	17 46 01.8	+67 27 09	8.0	14.74	15.28	0.33	0.2146	AGN1	
RX J1746.1+6737	2700	17 46 09.6	+67 37 21	17 46 08.8	+67 37 15	33.3	175.86	182.34	0.14	0.0410	AGN1	n
RX J1746.2+6627	2740	17 46 14.4	+66 27 39	17 46 15.1	+66 27 48	5.8	5.18	5.37	...	...	Star	
RX J1746.2+6227	2710	17 46 14.6	+62 27 01	17 46 13.9	+62 26 54	9.4	36.38	37.73	465.51	3.8890	AGN1	n
RX J1746.3+6320	2750	17 46 21.6	+63 20 06	17 46 21.8	+63 20 10	6.3	18.54	19.23	1.32	0.3697	AGN1	
RX J1746.7+6639	2770	17 46 45.0	+66 39 20	17 46 46.8	+66 39 04	4.8	7.12	8.81	0.60	0.3864	CL	sc = 1.237
RX J1746.7+7047	2780	17 46 45.5	+70 47 01	17 46 44.8	+70 47 03	7.7	12.80	13.27	...	...	Star K-M	
RX J1747.0+6836	2800	17 47 00.3	+68 36 26	17 46 59.9	+68 36 34	35.5	258.46	267.99	0.47	0.0630	AGN1	n
RX J1747.1+6813	2810	17 47 10.6	+68 13 19	17 47 12.7	+68 13 26	4.4	6.95	7.21	29.81	2.3920	AGN1	
RX J1747.2+6532	2820	17 47 14.4	+65 32 30	17 47 13.9	+65 32 35	6.8	12.61	13.08	19.47	1.5166	AGN1	
RX J1747.3+6702	2840	17 47 22.2	+67 02 06	17 47 21.5	+67 02 01	6.0	8.04	8.34	2.56	0.7421	AGN1	
RX J1747.4+6626	2850	17 47 26.8	+66 26 27	17 47 27.0	+66 26 24	9.9	16.22	16.82	0.15	0.1391	AGN1	n
RX J1747.4+6924	2860	17 47 27.0	+69 24 55	17 47 27.9	+69 25 09	4.9	11.45	11.87	1.75	0.5292	AGN2	
RX J1747.5+6343	2870	17 47 33.6	+63 43 55	17 47 31.1	+63 45 23	5.1	12.52	15.71	0.76	0.3280	CL	sc = 1.255
RX J1747.9+6623	2880	17 47 57.4	+66 23 27	17 47 58.5	+66 23 26	9.8	15.54	21.46	0.29	0.1738	GAL	n
RX J1747.9+6538	2890	17 47 58.0	+65 38 35	17 47 57.9	+65 38 28	13.9	35.98	37.31	1.94	0.3248	AGN1	
RX J1748.2+7016	2900	17 48 17.4	+70 16 14	17 48 19.6	+70 16 09	12.4	52.84	54.79	0.89	0.1858	AGN1	
RX J1748.3+6403	2910	17 48 22.7	+64 03 27	17 48 23.1	+64 03 38	6.7	17.70	18.35	10.50	0.9859	AGN1	
RX J1748.4+6335	2920	17 48 28.7	+63 35 41	17 48 29.3	+63 35 51	12.8	28.28	29.32	...	...	Star	
RX J1748.5+7005	2930	17 48 32.9	+70 05 51	17 48 32.9	+70 05 51	15.6	70.12	72.70	24.18	0.7700	BL	n
RX J1748.5+6308	2931	17 48 33.6	+63 08 39	17 48 33.7	+63 08 45	4.3	4.88	5.06	...	...	Star G	
RX J1748.6+6842	2940	17 48 38.8	+68 42 11	17 48 38.3	+68 42 17	10.3	28.40	29.44	0.04	0.0537	AGN1	n
RX J1748.6+7020	2950	17 48 41.6	+70 20 31	17 48 39.1	+70 20 42	5.2	11.09	13.84	0.74	0.3450	CL	sc = 1.249
RX J1749.0+6247	2970	17 49 02.7	+62 47 44	17 49 03.9	+62 47 48	11.8	27.38	28.39	...	...	Star F2	HD 162898
RX J1749.0+7014	2980	17 49 03.5	+70 14 42	17 49 04.5	+70 14 45	7.2	19.76	23.79	3.41	0.5790	CL	sc = 1.204
RX J1749.3+6737	2990	17 49 18.6	+67 37 24	17 49 18.0	+67 37 29	6.5	4.23	4.38	...	...	Star	
RX J1749.3+6411	3000	17 49 20.4	+64 11 08	17 49 19.5	+64 11 19	5.7	12.45	12.91	7.35	0.9836	AGN1	
RX J1749.7+6422	3001	17 49 42.4	+64 22 46	17 49 44.1	+64 22 58	4.6	8.89	9.22	2.93	0.7540	AGN1	
RX J1749.8+6823	3030	17 49 49.8	+68 23 15	17 49 54.5	+68 24 25	6.1	9.46	22.07	0.03	0.0508	CL	sc = 2.332
RX J1749.9+6611	3040	17 49 55.0	+66 11 16	17 49 55.9	+66 11 08	4.9	2.32	2.41	...	...	Star	
RX J1750.2+6814	3050	17 50 14.3	+68 14 33	17 50 16.1	+68 14 37	5.3	8.40	8.71	0.22	0.2310	AGN1	
RX J1750.2+6207	3070	17 50 15.3	+62 07 41	17 50 15.0	+62 07 56	7.1	12.20	12.65	...	...	Star	
RX J1750.2+6415	3060	17 50 15.5	+64 15 15	17 50 15.1	+64 14 56	6.1	13.01	13.49	0.41	0.2504	AGN2	
RX J1750.4+7045	3080	17 50 24.9	+70 45 37	17 50 25.3	+70 45 36	25.4	92.09	95.49	...	...	Star K5 IV	
RX J1751.0+6710	3100	17 51 02.4	+67 10 09	17 51 01.2	+67 10 14	4.8	4.59	4.76	0.88	0.5870	AGN1	
RX J1751.1+6753	3120	17 51 09.5	+67 53 07	17 51 08.9	+67 53 08	5.6	7.53	7.81	0.45	0.3406	AGN1	
RX J1751.2+6533	3121	17 51 15.5	+65 33 33	17 51 07.5	+65 31 50	6.1	8.48	22.83	0.02	0.0424	CL	sc = 2.691, n
RX J1751.5+7013	3130	17 51 30.7	+70 13 32	17 51 32.6	+70 13 22	5.2	10.79	13.10	1.41	0.4925	CL	sc = 1.215, n
RX J1751.5+6719	10	17 51 30.9	+67 19 20	17 51 31.1	+67 19 17	9.3	13.86	23.04	0.09	0.0933	CL	sc = 1.663
RX J1751.6+6540	3160	17 51 39.7	+65 40 40	17 51 36.9	+65 40 30	8.1	14.57	15.11	5.86	0.8259	AGN1	
RX J1751.8+6414	3161	17 51 50.8	+64 14 58	17 51 49.2	+64 15 01	4.6	4.41	4.57	...	...	Star	
RX J1751.9+6551	3190	17 51 57.6	+65 51 20	17 51 56.7	+65 51 17	10.1	14.48	15.01	1.15	0.3901	AGN1	

TABLE 3—*Continued*

Object (1)	NEP Scan No. (2)	α_X (J2000) (3)	δ_X (J2000) (4)	α_{opt} (J2000) (5)	δ_{opt} (J2000) (6)	S/N (7)	$f_{X, det}$ (10^{-14}) (8)	$f_{X, tot}$ (10^{-14}) (9)	L_X (10^{44}) (10)	z (11)	ID (12)	Notes (13)
RX J1752.2+6522	3200	17 52 12.0	+65 22 22	17 52 08.2	+65 22 53	5.0	5.21	6.44	0.46	0.3923	CL	sc = 1.235, n
RX J1752.2+6624	3210	17 52 12.6	+66 24 56	17 52 11.7	+66 24 54	6.1	5.79	6.00	0.49	0.4002	AGN1	
RX J1752.7+6700	20	17 52 43.9	+67 00 24	17 52 44.8	+67 00 20	5.4	2.26	2.35	...	...	Star	
RX J1752.7+6738	30	17 52 45.6	+67 38 37	17 52 44.6	+67 38 31	5.8	3.10	3.21	...	...	Star	
RX J1752.7+6804	31	17 52 47.0	+68 04 48	17 52 45.6	+68 05 00	4.4	2.08	2.16	...	...	Star	
RX J1752.9+6625	3220	17 52 56.0	+66 25 15	17 52 56.0	+66 25 10	10.8	5.12	5.31	...	...	Star K0	SAO 17671
RX J1752.9+6440	3230	17 52 57.4	+64 40 58	17 52 56.9	+64 40 56	7.8	14.23	14.76	0.10	0.1230	AGN1	
RX J1753.1+6746	40	17 53 09.7	+67 46 44	17 53 09.6	+67 46 32	6.4	8.62	8.94	6.91	1.1297	AGN1	
RX J1753.5+6811	3231	17 53 30.9	+68 11 47	17 53 32.4	+68 12 01	4.0	6.96	7.22	0.70	0.4366	AGN2	
RX J1753.6+6542	3260	17 53 41.6	+65 42 42	17 53 42.1	+65 42 40	8.4	9.18	9.52	0.09	0.1400	AGN1	
RX J1753.8+6852	3270	17 53 51.4	+68 52 19	17 53 51.5	+68 52 28	4.6	3.87	4.01	...	...	Star	
RX J1753.9+7016	3280	17 53 55.5	+70 16 47	17 53 56.6	+70 16 42	5.3	11.43	11.85	0.02	0.0620	AGN1	n
RX J1754.0+6452	3300	17 54 05.3	+64 52 01	17 54 08.6	+64 53 30	4.8	6.66	8.64	0.24	0.2460	CL	sc = 1.298, n
RX J1754.0+6613	60	17 54 05.4	+66 13 54	17 54 04.8	+66 13 50	15.2	18.18	18.85	1.58	0.4067	AGN1	
RX J1754.1+6948	3310	17 54 07.9	+69 48 33	17 54 07.8	+69 48 26	7.2	8.63	8.95	...	...	Star	
RX J1754.5+6904	3320	17 54 35.0	+69 04 58	17 54 34.2	+69 05 07	4.7	6.09	7.39	0.88	0.5113	CL	sc = 1.212
RX J1754.6+6803	3330	17 54 41.9	+68 03 33	17 54 38.9	+68 03 28	35.3	167.51	303.61	0.78	0.0770	CL	sc = 1.812, n
RX J1754.7+6819	3340	17 54 42.3	+68 19 08	17 54 42.0	+68 19 06	6.0	8.28	8.58	0.46	0.3292	AGN1	
RX J1754.7+6208	3350	17 54 43.2	+62 08 21	17 54 42.3	+62 08 30	6.1	16.93	17.56	0.88	0.3190	AGN1	
RX J1754.7+6623	90	17 54 45.7	+66 23 53	17 54 45.7	+66 23 49	14.7	13.47	22.96	0.08	0.0879	CL	sc = 1.704
RX J1754.8+6706	100	17 54 49.3	+67 06 00	17 54 49.7	+67 05 56	4.6	2.80	2.91	1.42	0.9190	AGN1	
RX J1755.0+6446	3360	17 55 00.0	+64 46 32	17 55 00.8	+64 46 32	6.5	9.83	10.20	2.64	0.6870	AGN1	
RX J1755.0+6235	3361	17 55 03.6	+62 35 30	17 55 03.2	+62 35 41	4.2	9.51	9.86	17.99	1.6607	AGN1	
RX J1755.0+6519	3370	17 55 05.8	+65 19 50	17 55 05.6	+65 19 55	31.6	111.44	115.55	0.32	0.0785	AGN1	
RX J1755.1+6719	110	17 55 09.0	+67 19 50	17 55 08.3	+67 19 54	6.1	6.02	6.24	0.15	0.2225	AGN2	
RX J1755.1+6852	3380	17 55 11.9	+68 52 30	17 55 10.7	+68 52 34	5.2	7.57	7.85	9.23	1.3645	AGN1	
RX J1755.3+6504	3390	17 55 19.9	+65 04 55	17 55 20.6	+65 04 47	7.0	8.14	14.10	0.04	0.0846	CL	sc = 1.733
RX J1755.3+6416	3391	17 55 21.7	+64 16 39	17 55 17.4	+64 16 29	6.2	9.27	11.81	0.43	0.2837	CL	sc = 1.274
RX J1755.6+6209	3420	17 55 40.3	+62 09 41	17 55 40.3	+62 09 39	8.9	27.64	28.66	0.09	0.0846	AGN2	
RX J1755.6+7009	3410	17 55 40.5	+70 09 52	17 55 41.3	+70 09 51	4.8	9.26	9.61	0.90	0.4295	AGN1	
RX J1755.7+6752	3411	17 55 45.5	+67 52 42	17 55 43.2	+67 54 09	18.8	57.31	100.02	0.30	0.0833	CL	sc = 1.745
RX J1755.7+6249	3430	17 55 46.2	+62 49 27	17 55 45.9	+62 49 29	11.8	46.07	47.77	1.27	0.2360	AGN1	
RX J1755.8+6236	3440	17 55 48.3	+62 36 41	17 55 48.4	+62 36 44	15.7	64.15	272.84	0.09	0.0270	CL	sc = 4.253
RX J1755.9+6314	3450	17 55 56.5	+63 14 03	17 55 57.8	+63 14 09	6.7	14.49	17.92	1.18	0.3850	CL	sc = 1.237
RX J1755.9+6540	140	17 55 56.9	+65 40 54	17 55 56.8	+65 40 52	9.9	10.66	11.05	0.57	0.3238	AGN1	
RX J1756.1+6615	160	17 56 10.0	+66 15 14	17 56 09.5	+66 15 09	12.3	10.23	10.60	2.32	0.6357	AGN1	
RX J1756.1+7001	3460	17 56 10.8	+70 01 55	17 56 11.9	+70 01 47	5.3	10.64	11.04	0.24	0.2129	AGN1	
RX J1756.1+7055	3470	17 56 10.8	+70 55 48	17 56 11.6	+70 55 50	7.4	19.61	20.34	0.59	0.2460	AGN1	
RX J1756.2+6619	170	17 56 12.0	+66 19 47	17 56 12.2	+66 19 46	5.8	2.73	2.84	2.21	1.1340	AGN1	
RX J1756.2+6955	3480	17 56 12.7	+69 55 21	17 56 12.7	+69 55 20	7.7	20.86	21.63	0.07	0.0838	AGN2	
RX J1756.2+6838	3490	17 56 13.6	+68 38 31	17 56 15.5	+68 38 25	5.8	8.78	9.11	0.04	0.1019	AGN2	spiral
RX J1756.2+6807	3500	17 56 14.0	+68 07 07	17 56 14.0	+68 07 09	17.7	23.22	24.07	...	...	Star	
RX J1756.2+7042	3501	17 56 14.2	+70 42 46			6.6	19.19	19.90	...	...		n
RX J1756.4+6300	3510	17 56 25.2	+63 00 42	17 56 25.4	+63 00 49	4.8	8.93	9.25	6.90	1.1110	AGN1	
RX J1756.5+6513	3520	17 56 31.0	+65 13 01	17 56 29.3	+65 12 48	8.4	11.26	45.27	0.02	0.0284	CL	sc = 4.020
RX J1756.7+6438	3530	17 56 43.2	+64 38 53	17 56 43.4	+64 38 59	12.2	26.72	27.71	0.66	0.2233	AGN1	
RX J1756.8+6612	180	17 56 52.4	+66 12 42	17 56 51.3	+66 12 42	10.2	7.30	7.57	9.82	1.4252	AGN1	

TABLE 3—*Continued*

Object (1)	NEP Scan No. (2)	α_X (J2000) (3)	δ_X (J2000) (4)	α_{opt} (J2000) (5)	δ_{opt} (J2000) (6)	S/N (7)	$f_{X, det}$ (10^{-14}) (8)	$f_{X, tot}$ (10^{-14}) (9)	L_X (10^{44}) (10)	z (11)	ID (12)	Notes (13)
RX J1756.9+6238	3550	17 56 58.2	+62 38 44	17 57 00.6	+62 38 55	7.9	23.49	24.36	17.41	1.0902	AGN1	
RX J1757.0+6849	3560	17 57 03.6	+68 49 23	17 57 03.7	+68 49 14	11.5	15.00	15.55	...	...	Star K0	HD 164781
RX J1757.1+6352	3570	17 57 09.7	+63 52 38	17 57 09.5	+63 52 33	7.6	16.60	17.21	0.88	0.3220	AGN1	
RX J1757.2+7033	3580	17 57 12.7	+70 33 39	17 57 13.2	+70 33 38	42.0	409.45	424.56	35.64	0.4070	BL	n
RX J1757.2+6547	190	17 57 13.8	+65 47 02	17 57 14.3	+65 46 58	9.4	3.93	4.07	...	...	Star M	n
RX J1757.3+6631	200	17 57 19.8	+66 31 39	17 57 19.4	+66 31 31	7.8	3.24	3.87	0.86	0.6909	CL	sc = 1.195, n
RX J1757.5+6841	3590	17 57 34.1	+68 41 22	17 57 34.1	+68 41 21	11.4	25.93	26.89	0.41	0.1814	AGN1	
RX J1757.9+6934	3600	17 57 55.2	+69 34 23	17 57 55.2	+69 34 25	11.2	32.64	33.85	0.10	0.0795	AGN1	
RX J1757.9+6609	210	17 57 56.9	+66 09 23	17 57 56.5	+66 09 20	5.0	3.01	3.12	0.38	0.4865	AGN2	n
RX J1758.0+6409	3610	17 58 01.0	+64 09 32	17 58 01.4	+64 09 34	21.2	40.36	41.85	...	...	Star G	SAO 17709
RX J1758.0+6851	3620	17 58 02.4	+68 51 46	17 58 03.7	+68 51 51	4.7	7.54	7.82	0.13	0.1876	AGN1	
RX J1758.2+7020	3621	17 58 12.4	+70 20 27	17 58 13.4	+70 20 23	4.4	9.63	9.98	7.87	1.1400	AGN1	
RX J1758.2+6743	230	17 58 13.2	+67 43 18	17 58 14.1	+67 43 17	10.2	15.18	15.74	0.31	0.2045	AGN1	
RX J1758.3+6906	3630	17 58 18.7	+69 06 30	17 58 15.9	+69 06 32	6.5	12.62	13.08	42.89	2.1572	AGN1	
RX J1758.3+6735	240	17 58 19.1	+67 35 15	17 58 18.9	+67 35 15	5.0	1.79	1.85	...	...	Star	
RX J1758.3+6203	241	17 58 23.3	+62 03 26	17 58 24.4	+62 03 20	4.1	8.98	9.32	2.21	0.6590	AGN1	
RX J1758.4+6531	250	17 58 24.1	+65 31 05	17 58 24.2	+65 31 08	15.0	23.22	24.08	1.25	0.3250	AGN1	
RX J1758.4+6726	260	17 58 28.8	+67 26 08	17 58 28.3	+67 26 08	7.8	2.80	2.90	...	...	Star	
RX J1758.5+6637	270	17 58 33.4	+66 37 59	17 58 33.1	+66 37 57	11.8	5.96	6.18	...	...	PN	
RX J1758.7+6423	3680	17 58 44.5	+64 23 04	17 58 43.1	+64 23 04	4.9	6.21	6.44	2.03	0.7523	AGN1	
RX J1758.7+6350	3690	17 58 47.2	+63 50 39	17 58 48.0	+63 50 39	12.1	18.04	18.70	...	...	Star A2	HD 164873
RX J1758.8+6551	280	17 58 52.8	+65 51 06	17 58 53.2	+65 51 13	6.0	3.64	3.77	0.29	0.3884	AGN2	
RX J1758.9+6211	281	17 58 54.3	+62 11 26	17 58 54.1	+62 11 24	5.4	7.38	7.65	...	...	Star M	
RX J1758.9+6220	3700	17 58 56.5	+62 20 31	17 58 56.3	+62 20 25	4.1	8.02	8.32	2.18	0.6910	AGN1	
RX J1758.9+6520	310	17 58 57.6	+65 20 58	17 58 56.5	+65 21 05	5.0	3.65	4.53	0.28	0.3652	CL	sc = 1.242, n
RX J1759.2+6408	3710	17 59 12.5	+64 08 33	17 59 13.8	+64 08 33	15.9	24.59	25.49	...	...	Star F2	HD 164984
RX J1759.2+6902	3720	17 59 17.5	+69 02 20	17 59 15.0	+69 02 59	6.0	10.34	16.77	0.07	0.0994	CL	sc = 1.622
RX J1759.3+6335	3730	17 59 19.2	+63 35 37	17 59 18.4	+63 35 40	4.5	7.14	7.41	6.98	1.2354	AGN1	
RX J1759.3+6602	330	17 59 23.4	+66 02 53	17 59 23.6	+66 02 55	6.0	1.79	1.85	...	...	Star	
RX J1759.7+6739	350	17 59 42.5	+67 39 25	17 59 42.8	+67 39 27	7.0	6.17	6.40	4.51	1.0830	AGN1	
RX J1759.7+6629	360	17 59 44.3	+66 29 11	17 59 44.7	+66 29 11	10.0	4.78	4.96	0.40	0.3990	AGN1	n
RX J1759.8+7037	3760	17 59 49.3	+70 37 19	17 59 49.3	+70 37 19	21.8	125.61	130.25	...	...	BL	
RX J1800.0+6645	370	18 00 01.8	+66 45 59	18 00 02.2	+66 45 53	7.0	1.25	1.30	...	...	Star G-K	n
RX J1800.1+6636	380	18 00 07.5	+66 36 54	18 00 07.6	+66 36 55	12.0	5.75	5.97	0.002	0.0260	AGN2	n, NGC6552, spiral
RX J1800.1+6938	381	18 00 08.4	+69 38 30	18 00 10.4	+69 38 38	4.2	6.71	6.96	4.72	1.0650	AGN1	
RX J1800.1+6835	3790	18 00 09.9	+68 35 57	18 00 10.0	+68 35 56	75.8	333.84	346.16	...	...	Star O	KUV 18004+6836
RX J1800.1+6720	390	18 00 11.2	+67 20 48	18 00 10.9	+67 20 58	6.0	4.42	4.58	3.64	1.1433	AGN1	
RX J1800.3+6615	430	18 00 23.1	+66 15 54	18 00 23.8	+66 15 52	9.6	5.71	5.93	0.61	0.4475	AGN1	
RX J1800.3+6349	3800	18 00 23.9	+63 49 53	18 00 24.3	+63 49 53	13.0	17.86	18.52	...	...	Star	
RX J1800.4+7051	3810	18 00 25.2	+70 51 55	18 00 25.8	+70 51 58	5.3	12.15	12.60	0.63	0.3200	AGN1	
RX J1800.4+6357	3820	18 00 26.2	+63 57 19	18 00 26.4	+63 57 19	10.2	22.56	23.39	5.99	0.6828	AGN1	
RX J1800.4+6913	3830	18 00 28.2	+69 13 22	18 00 33.4	+69 13 20	16.6	63.16	110.99	0.33	0.0821	CL	sc = 1.757, A 2295
RX J1800.4+6705	440	18 00 29.0	+67 05 48	18 00 28.9	+67 05 50	8.2	4.99	5.18	5.78	1.3330	AGN1	
RX J1800.9+6600	470	18 00 57.6	+66 00 58	18 00 57.4	+66 00 56	10.7	3.81	3.95	...	...	Star	
RX J1801.2+6433	3860	18 01 13.2	+64 33 22	18 01 14.7	+64 33 26	5.5	7.03	7.29	3.17	0.8700	AGN1	
RX J1801.2+6902	3870	18 01 14.6	+69 02 43	18 01 14.6	+69 02 43	4.8	7.05	7.31	7.33	1.2700	AGN1	n
RX J1801.2+6624	480	18 01 15.2	+66 24 01	18 01 16.6	+66 24 01	6.0	1.43	1.48	1.44	1.2500	AGN1	n

TABLE 3—*Continued*

Object (1)	NEP Scan No. (2)	α_X (J2000) (3)	δ_X (J2000) (4)	α_{opt} (J2000) (5)	δ_{opt} (J2000) (6)	S/N (7)	$f_{X, det}$ (10^{-14}) (8)	$f_{X, tot}$ (10^{-14}) (9)	L_X (10^{44}) (10)	z (11)	ID (12)	Notes (13)
RX J1801.3+6654	500	18 01 21.6	+66 54 05	18 01 21.9	+66 54 04	26.5	15.78	16.36	...	...	Star K	
RX J1801.4+6800	501	18 01 26.9	+68 00 27	18 01 26.7	+68 00 30	4.4	2.08	2.16	...	...	Star	
RX J1801.7+6638	510	18 01 46.7	+66 38 39	18 01 47.0	+66 38 40	27.6	29.81	30.91	...	...	BL	n
RX J1802.0+6629	560	18 02 05.9	+66 29 02	18 02 04.8	+66 29 14	4.3	1.56	1.61	0.05	0.2650	AGN1	n
RX J1802.1+6535	570	18 02 07.7	+65 35 21	18 02 07.7	+65 35 14	4.9	4.09	4.24	0.04	0.1513	AGN1	
RX J1802.2+6415	3900	18 02 16.2	+64 15 46	18 02 15.2	+64 16 03	33.5	85.66	88.82	...	...	Star	G 227-22
RX J1802.3+6259	3910	18 02 19.6	+62 59 21	18 02 21.5	+62 59 14	4.5	7.28	7.55	2.20	0.7240	AGN1	
RX J1802.3+6647	590	18 02 22.8	+66 47 49	18 02 24.5	+66 47 35	9.4	5.65	5.86	0.34	0.3424	AGN1	
RX J1802.7+6727	630	18 02 47.4	+67 27 50	18 02 47.8	+67 27 41	4.3	3.22	3.34	0.04	0.1620	AGN2	n, spiral
RX J1802.8+6605	640	18 02 51.2	+66 05 40	18 02 51.3	+66 05 42	18.4	19.85	20.58	0.42	0.2070	AGN1	
RX J1802.9+6339	3940	18 02 54.0	+63 39 10	18 02 54.6	+63 39 10	4.2	4.91	8.26	0.03	0.0907	CL	sc = 1.682
RX J1803.0+6445	3970	18 03 05.7	+64 45 26	18 03 05.8	+64 45 29	10.7	10.83	11.23	...	...	Star M	
RX J1803.4+6738	650	18 03 28.3	+67 38 06	18 03 29.0	+67 38 10	66.7	346.31	359.09	3.05	0.1360	AGN1	n, Kazarian 102
RX J1803.4+6437	3990	18 03 29.5	+64 37 41	18 03 33.6	+64 37 47	4.8	3.45	3.58	...	...	Star M	
RX J1803.8+6619	660	18 03 50.4	+66 19 31	18 03 50.1	+66 19 31	10.7	7.72	8.00	0.64	0.3968	AGN1	
RX J1803.9+6548	670	18 03 54.5	+65 48 27	18 03 54.3	+65 48 25	15.7	18.84	19.54	0.06	0.0850	BL	n
RX J1804.2+6754	680	18 04 13.3	+67 54 11	18 04 14.0	+67 54 11	9.3	6.67	6.91	...	...	Star CV	
RX J1804.2+6729	690	18 04 15.6	+67 29 21	18 04 13.6	+67 29 31	4.7	3.41	6.98	0.01	0.0617	CL	sc = 2.047
RX J1804.3+6629	700	18 04 18.7	+66 29 54	18 04 24.7	+66 29 28	5.5	1.31	1.36	...	...	Star	n
RX J1804.5+6429	4010	18 04 32.5	+64 29 10	18 04 32.9	+64 29 03	5.7	4.05	4.20	...	...	Star M	
RX J1804.5+6937	4020	18 04 34.2	+69 37 33	18 04 34.4	+69 37 37	5.1	10.10	10.47	2.06	0.6055	AGN1	
RX J1804.6+6528	4121	18 04 39.0	+65 28 59	18 04 38.6	+65 28 58	7.7	4.11	4.26	...	...	Star	
RX J1804.6+6846	4040	18 04 41.9	+68 46 02	18 04 40.6	+68 45 55	5.5	8.98	9.31	0.04	0.0969	AGN2	
RX J1805.1+6353	4060	18 05 07.1	+63 53 26	18 05 08.4	+63 53 35	5.8	5.54	5.74	...	...	Star M	
RX J1805.2+7006	4080	18 05 16.6	+70 06 19	18 05 17.8	+70 06 22	6.8	19.44	20.15	0.33	0.1874	AGN1	
RX J1805.4+6638	710	18 05 25.3	+66 38 58	18 05 25.0	+66 39 03	13.1	12.54	13.01	0.13	0.1449	AGN1	
RX J1805.5+6945	4090	18 05 30.0	+69 45 06	18 05 30.5	+69 45 17	9.7	15.00	15.55	...	...	Star	
RX J1805.5+6219	4100	18 05 30.4	+62 19 04	18 05 30.3	+62 19 03	5.2	5.89	6.11	...	...	Star K0	HD 166227
RX J1805.6+6624	720	18 05 36.1	+66 24 52	18 05 36.2	+66 24 52	13.8	13.14	13.63	3.93	0.7210	AGN1	
RX J1805.6+6309	4110	18 05 39.0	+63 09 36	18 05 40.1	+63 09 22	5.0	8.98	9.32	1.22	0.5013	AGN1	
RX J1805.6+6432	4120	18 05 41.4	+64 32 51	18 05 40.5	+64 32 47	8.1	13.88	14.39	4.43	0.7432	AGN1	
RX J1805.7+6551	4130	18 05 45.9	+65 51 55	18 05 44.8	+65 51 58	7.8	3.69	3.83	...	...	Star F5	SAO 17761
RX J1806.0+6940	4140	18 06 03.2	+69 40 26	18 06 03.2	+69 40 24	5.1	10.71	11.11	0.56	0.3214	AGN1	
RX J1806.1+6813	4150	18 06 06.6	+68 13 08	18 06 04.8	+68 13 16	8.8	15.75	19.91	0.81	0.3030	CL	sc = 1.265, n
RX J1806.2+6644	740	18 06 12.5	+66 44 40	18 06 12.4	+66 44 34	6.8	4.87	5.05	0.30	0.3482	AGN1	
RX J1806.3+6524	4160	18 06 22.2	+65 24 15	18 06 21.8	+65 24 06	5.4	3.51	3.64	...	...	Star	
RX J1806.4+7028	4170	18 06 24.9	+70 28 40	18 06 25.5	+70 28 48	8.0	26.66	43.64	0.18	0.0971	GAL	n
RX J1806.6+6413	4180	18 06 40.7	+64 13 05	18 06 41.0	+64 13 18	5.2	3.99	4.14	...	...	Star K0	HD 166578
RX J1806.7+6822	4190	18 06 43.3	+68 22 00	18 06 43.6	+68 22 01	11.7	13.27	13.76	...	...	Star M	
RX J1806.7+6626	750	18 06 47.4	+66 26 18	18 06 47.0	+66 26 07	9.3	3.87	4.01	...	...	Star M	
RX J1806.8+6949	4200	18 06 50.2	+69 49 23	18 06 50.6	+69 49 28	27.0	185.38	192.22	0.22	0.0508	BL	n
RX J1806.8+6537	4210	18 06 51.6	+65 37 46	18 06 52.6	+65 37 44	14.3	24.73	31.80	0.96	0.2626	CL	sc = 1.286
RX J1807.0+6643	4211	18 07 00.5	+66 43 48	18 06 58.2	+66 43 30	10.6	5.66	5.86	...	...	Star M	
RX J1807.3+6635	4240	18 07 19.3	+66 35 30	18 07 19.9	+66 35 29	19.2	12.56	13.02	...	...	Star K	
RX J1807.5+6429	4250	18 07 32.3	+64 29 17	18 07 32.2	+64 29 26	4.7	6.61	8.61	0.22	0.2391	CL	sc = 1.304
RX J1807.6+6829	4260	18 07 39.6	+68 29 17	18 07 39.7	+68 29 22	9.6	10.89	11.30	...	...	Star	
RX J1807.7+6617	4270	18 07 47.4	+66 17 32	18 07 47.4	+66 17 31	10.9	10.31	10.69	5.44	0.9350	AGN1	

TABLE 3—*Continued*

Object (1)	NEP Scan No. (2)	α_X (J2000) (3)	δ_X (J2000) (4)	α_{opt} (J2000) (5)	δ_{opt} (J2000) (6)	S/N (7)	$f_{X,det}$ (10^{-14}) (8)	$f_{X,tot}$ (10^{-14}) (9)	L_X (10^{44}) (10)	z (11)	ID (12)	Notes (13)
RX J1808.0+6452	4280	18 08 02.5	+64 52 24	18 08 03.7	+64 52 30	10.0	24.25	25.14	16.05	1.0360	AGN1	
RX J1808.4+6437	4281	18 08 25.2	+64 37 24	18 08 23.7	+64 37 12	5.6	5.71	5.93	...	...	Star	
RX J1808.5+6643	4310	18 08 35.6	+66 43 22	18 08 35.3	+66 43 22	8.1	3.39	3.52	...	...	Star	
RX J1808.6+6735	4350	18 08 40.7	+67 35 53	18 08 41.6	+67 36 00	13.2	14.11	14.63	...	...	Star	
RX J1808.7+6557	4370	18 08 43.6	+65 57 05	18 08 43.1	+65 57 05	6.6	5.50	7.14	0.20	0.2460	CL	sc = 1.298
RX J1808.7+6256	4380	18 08 45.3	+62 56 31	18 08 45.4	+62 56 37	6.7	9.17	9.51	...	...	Star G5	HD 166975
RX J1808.8+6634	4390	18 08 49.8	+66 34 31	18 08 49.6	+66 34 29	16.9	25.96	26.92	7.20	0.6970	AGN1	n
RX J1808.8+6530	4400	18 08 51.0	+65 30 21	18 08 50.8	+65 30 19	7.3	11.24	11.65	0.49	0.2937	AGN2	
RX J1808.8+6511	4401	18 08 53.4	+65 11 42	18 08 53.5	+65 11 48	4.3	5.06	5.25	9.25	1.6350	AGN1	
RX J1809.0+6704	4410	18 09 01.0	+67 04 21	18 09 00.9	+67 04 25	5.8	5.49	5.70	1.51	0.6950	AGN1	
RX J1809.0+6800	4420	18 09 03.5	+68 00 55	18 09 03.1	+68 00 57	5.2	7.54	7.82	1.48	0.5946	AGN1	
RX J1809.0+6333	4430	18 09 05.0	+63 33 00	18 09 05.5	+63 33 09	4.3	8.00	8.29	1.85	0.6412	AGN1	
RX J1809.5+6620	4440	18 09 30.1	+66 20 33	18 09 30.1	+66 20 21	6.8	7.20	7.47	1.63	0.6350	AGN1	
RX J1809.5+6609	4450	18 09 34.8	+66 09 06	18 09 34.2	+66 09 11	6.1	6.49	6.73	3.47	0.9400	AGN1	
RX J1809.7+6837	4460	18 09 46.8	+68 37 26	18 09 48.4	+68 37 34	4.9	7.44	7.71	0.17	0.2173	AGN1	
RX J1809.9+6940	4470	18 09 54.5	+69 40 46	18 09 55.8	+69 40 39	27.9	101.14	104.87	...	...	Star K2	HD 167605
RX J1810.0+6344	4490	18 10 04.2	+63 44 24	18 10 04.4	+63 44 26	8.6	24.63	25.53	1.82	0.3770	AGN1	
RX J1810.1+6728	4500	18 10 06.3	+67 28 33	18 10 08.0	+67 28 35	4.4	2.08	2.16	...	...	Star	
RX J1810.3+6328	4501	18 10 23.5	+63 28 08	18 10 16.9	+63 29 14	5.4	14.88	15.43	6.17	0.8380	AGN1	n
RX J1810.4+6432	4520	18 10 24.7	+64 32 46	18 10 24.2	+64 32 54	4.5	7.58	7.86	0.35	0.3030	AGN1	
RX J1810.8+7016	4530	18 10 48.9	+70 16 00	18 10 49.9	+70 16 09	13.6	33.22	34.44	...	...	Star	
RX J1811.2+6543	4550	18 11 12.4	+65 43 46	18 11 11.6	+65 43 47	9.1	15.05	15.61	1.94	0.4895	AGN1	
RX J1811.3+6447	4560	18 11 19.1	+64 47 36	18 11 19.3	+64 47 23	6.2	11.07	13.53	1.23	0.4510	CL	sc = 1.222
RX J1811.3+6314	4570	18 11 20.5	+63 14 45	18 11 21.5	+63 14 49	4.3	5.12	5.31	...	...	Star G	
RX J1811.6+6507	4580	18 11 36.8	+65 07 04	18 11 36.1	+65 07 00	9.9	23.01	23.86	9.78	0.8470	AGN1	
RX J1811.6+6333	4590	18 11 41.2	+63 33 46	18 11 43.5	+63 33 51	4.4	9.25	9.59	0.52	0.3310	AGN1	
RX J1812.1+6353	4610	18 12 08.4	+63 53 35	18 12 08.2	+63 53 32	6.3	14.28	17.25	2.20	0.5408	CL	sc = 1.208
RX J1812.4+6610	4640	18 12 27.0	+66 10 46	18 12 26.1	+66 10 48	4.5	4.25	4.41	1.00	0.6449	AGN1	
RX J1812.7+6533	4650	18 12 45.9	+65 33 47	18 12 44.6	+65 33 49	5.5	3.57	3.70	...	...	Star	
RX J1812.8+6946	4660	18 12 53.9	+69 46 22	18 12 54.3	+69 46 23	5.6	6.61	6.85	...	...	Star M	
RX J1813.0+6644	4670	18 13 04.8	+66 44 56	18 13 06.1	+66 44 52	5.6	6.83	7.09	2.34	0.7680	AGN1	
RX J1813.1+6547	4680	18 13 09.0	+65 47 01	18 13 07.7	+65 47 04	7.8	12.05	12.49	0.76	0.3489	AGN1	
RX J1813.1+6608	4690	18 13 10.7	+66 08 02	18 13 07.9	+66 08 09	5.0	5.30	5.50	6.21	1.3400	AGN1	
RX J1813.1+6230	4691	18 13 11.5	+62 30 33	18 13 15.4	+62 30 32	4.3	13.06	17.84	0.27	0.1829	CL	sc = 1.366
RX J1813.5+6635	4720	18 13 34.1	+66 35 36	18 13 35.1	+66 35 34	4.8	4.64	4.81	1.15	0.6609	AGN1	
RX J1813.6+6731	4721	18 13 41.5	+67 31 50	18 13 43.0	+67 32 23	7.5	17.42	18.06	3.70	0.6168	AGN1	
RX J1813.7+6628	4750	18 13 45.6	+66 28 49	18 13 47.0	+66 28 59	14.6	15.66	16.23	...	...	Star M	
RX J1813.7+6707	4770	18 13 46.2	+67 07 40	18 13 45.9	+67 07 41	5.1	3.04	3.15	...	...	Star	
RX J1813.7+6538	4760	18 13 46.6	+65 38 21	18 13 45.8	+65 38 20	15.5	40.46	41.96	0.72	0.1912	AGN1	
RX J1813.8+6831	4780	18 13 48.3	+68 31 21	18 13 48.6	+68 31 32	4.2	3.27	3.39	...	...	Star	
RX J1813.8+6728	4800	18 13 51.0	+67 28 10	18 13 50.7	+67 28 06	5.6	10.28	10.66	0.54	0.3196	AGN1	
RX J1813.8+6423	4810	18 13 53.7	+64 23 48	18 13 51.4	+64 23 57	34.1	144.24	149.56	...	...	Star F5	HR 6850
RX J1814.2+6939	4840	18 14 14.4	+69 39 33	18 14 20.2	+69 39 53	11.6	53.60	91.55	0.31	0.0874	CL	sc = 1.708, A2301
RX J1815.2+6658	4880	18 15 17.0	+66 58 10	18 15 17.4	+66 58 05	5.8	8.58	8.90	0.22	0.2287	AGN2	
RX J1815.3+6507	4890	18 15 19.1	+65 07 28	18 15 20.0	+65 07 14	4.9	8.61	8.93	17.69	1.7234	AGN1	
RX J1815.4+6806	4910	18 15 24.4	+68 06 29	18 15 24.9	+68 06 32	9.7	26.15	27.11	0.74	0.2390	AGN1	n
RX J1815.8+6441	4930	18 15 52.3	+64 41 00	18 15 51.7	+64 41 03	5.8	13.27	13.76	1.18	0.4116	AGN1	

TABLE 3—*Continued*

Object (1)	NEP Scan No. (2)	α_X (J2000) (3)	δ_X (J2000) (4)	α_{opt} (J2000) (5)	δ_{opt} (J2000) (6)	S/N (7)	$f_{X,det}$ (10^{-14}) (8)	$f_{X,tot}$ (10^{-14}) (9)	L_X (10^{44}) (10)	z (11)	ID (12)	Notes (13)
RX J1816.2+6529	4931	18 16 17.2	+65 29 48	18 16 21.2	+65 29 39	4.3	3.10	3.21	...	...	Star	
RX J1816.5+6911	4950	18 16 32.4	+69 11 34	18 16 29.6	+69 11 34	4.8	10.73	14.28	0.28	0.2097	CL	sc = 1.331
RX J1816.5+6547	4960	18 16 32.9	+65 47 00	18 16 32.3	+65 47 02	6.3	4.52	4.69	...	...	Star	
RX J1816.8+6504	4970	18 16 48.1	+65 04 29	18 16 49.7	+65 04 26	6.8	6.91	7.16	...	...	Star	
RX J1816.9+6449	4980	18 16 59.4	+64 49 09	18 16 58.6	+64 49 34	5.8	6.85	7.10	...	...	Star	
RX J1817.1+7024	4990	18 17 08.4	+70 24 13	18 17 10.3	+70 23 54	5.2	14.97	25.76	0.08	0.0859	CL	sc = 1.721
RX J1817.5+6631	5020	18 17 32.1	+66 31 08	18 17 31.3	+66 31 11	6.9	10.17	10.54	1.10	0.4513	AGN1	
RX J1817.7+6824	5030	18 17 46.1	+68 24 24	18 17 44.7	+68 24 24	15.0	59.48	75.81	2.59	0.2820	CL	sc = 1.275
RX J1818.4+6741	5050	18 18 28.9	+67 41 26	18 18 28.8	+67 41 24	25.6	137.81	142.89	6.92	0.3140	AGN1	
RX J1818.5+7042	5060	18 18 34.1	+70 42 15	18 18 31.9	+70 42 17	6.7	11.19	11.60	...	...	Star G5	SAO 9067
RX J1818.7+6518	5080	18 18 46.2	+65 18 14	18 18 44.8	+65 18 10	4.3	6.72	6.97	7.46	1.3080	AGN1	
RX J1818.9+6611	5090	18 18 57.2	+66 11 34	18 18 53.7	+66 11 54	18.7	33.40	34.63	...	...	Star M	
RX J1819.0+6909	5091	18 19 04.1	+69 09 24	18 18 58.8	+69 09 45	5.2	15.11	25.74	0.09	0.0880	CL	sc = 1.703
RX J1819.8+6748	5092	18 19 48.8	+67 48 48	18 19 48.3	+67 48 42	4.8	10.59	14.03	0.29	0.2153	CL	sc = 1.325
RX J1819.8+6510	5150	18 19 52.2	+65 10 35	18 19 51.5	+65 10 37	8.6	20.78	21.55	0.36	0.1894	AGN1	
RX J1819.9+6636	5170	18 19 55.4	+66 36 19	18 19 53.8	+66 36 19	8.0	7.14	7.41	...	...	Star	
RX J1819.9+6628	5190	18 19 59.9	+66 28 25	18 19 59.0	+66 28 30	4.1	6.04	6.26	6.32	1.2740	AGN1	
RX J1820.2+6857	5210	18 20 13.0	+68 57 22	18 20 25.9	+68 57 37	16.8	96.59	163.76	0.56	0.0890	CL	sc = 1.695, A 2304
RX J1820.3+6519	5220	18 20 19.7	+65 19 18	18 20 19.2	+65 19 19	19.6	40.84	42.34	...	...	Star F8	HD 69531
RX J1820.5+6620	5230	18 20 32.9	+66 20 29	18 20 32.9	+66 20 20	5.0	9.21	9.55	1.28	0.5057	AGN1	
RX J1820.5+6930	5240	18 20 35.3	+69 30 04	18 20 33.4	+69 30 15	6.4	20.95	21.72	0.43	0.2051	AGN1	
RX J1821.3+6559	5280	18 21 23.8	+65 59 27	18 21 25.0	+65 59 31	10.0	13.04	13.52	...	...	Star M	
RX J1821.6+6827	5281	18 21 38.1	+68 27 52	18 21 32.9	+68 27 55	4.6	8.60	10.22	2.91	0.8108	CL	sc = 1.189
RX J1821.6+6543	5300	18 21 38.8	+65 43 04	18 21 40.0	+65 43 10	8.6	20.59	21.35	0.73	0.2666	AGN2	
RX J1821.6+6328	5310	18 21 39.6	+63 28 27	18 21 38.8	+63 28 26	8.1	31.87	33.04	2.21	0.3656	AGN1	
RX J1821.7+6357	5320	18 21 46.6	+63 57 16	18 21 46.8	+63 57 10	5.4	8.04	8.33	...	...	Star	
RX J1821.9+6654	5321	18 21 55.7	+66 54 34	18 21 56.5	+66 54 26	5.1	6.98	7.24	0.02	0.0873	AGN1	
RX J1821.9+6420	5340	18 21 57.4	+64 20 51	18 21 57.1	+64 20 37	76.5	1258.14	1304.57	56.16	0.2970	AGN1	n
RX J1821.9+6818	5330	18 21 58.8	+68 18 42	18 21 59.4	+68 18 42	4.3	9.02	9.35	17.78	1.6920	AGN1	
RX J1822.6+6641	5370	18 22 37.4	+66 41 29	18 22 34.8	+66 41 21	6.1	10.10	17.14	0.06	0.0888	CL	sc = 1.697
RX J1823.1+6533	5380	18 23 08.8	+65 33 20	18 23 06.8	+65 33 14	5.4	4.46	4.63	...	...	Star F0	HD 170154
RX J1823.3+6419	5400	18 23 20.0	+64 19 23	18 23 19.2	+64 19 32	8.4	25.09	26.01	4.61	0.5766	AGN1	
RX J1823.4+6257	5410	18 23 27.0	+62 57 14	18 23 26.7	+62 57 18	4.9	8.75	9.07	...	...	Star	
RX J1823.6+6847	5411	18 23 38.6	+68 47 40	18 23 39.4	+68 47 46	4.5	10.90	11.31	0.23	0.2071	AGN1	
RX J1823.9+6719	5440	18 23 54.6	+67 19 41	18 23 54.7	+67 19 36	5.3	9.72	10.08	1.07	0.4536	AGN1	
RX J1824.5+6349	5480	18 24 31.5	+63 49 55	18 24 29.6	+63 49 37	6.9	14.76	15.31	...	...	Star	
RX J1824.7+6509	5500	18 24 46.9	+65 09 24	18 24 47.3	+65 09 25	26.4	75.54	78.33	...	...	Star	KUV 18246+6508
RX J1825.1+6450	5510	18 25 10.6	+64 50 17	18 25 09.0	+64 50 21	35.8	136.50	141.54	...	...	Star	HD 170527
RX J1825.5+6234	5520	18 25 33.4	+62 34 16	18 25 32.9	+62 34 15	17.7	78.99	81.91	...	...	Star	
RX J1825.7+6905	5530	18 25 46.3	+69 05 51	18 25 47.3	+69 05 54	10.1	47.68	49.44	0.18	0.0888	AGN1	
RX J1826.6+6706	5550	18 26 38.3	+67 06 47	18 26 37.5	+67 06 44	9.2	26.84	27.83	1.11	0.2870	AGN1	n
RX J1827.2+6549	5560	18 27 15.3	+65 49 21	18 27 13.9	+65 49 20	4.4	8.93	9.26	8.57	1.2250	AGN1	
RX J1827.5+6431	5590	18 27 33.6	+64 31 38	18 27 33.8	+64 31 44	6.4	16.89	17.52	0.08	0.0977	AGN1	
RX J1827.9+6235	5600	18 27 58.1	+62 35 36	18 27 57.0	+62 35 41	5.7	10.77	11.17	...	...	Star	
RX J1828.1+6709	5601	18 28 06.6	+67 09 23	18 28 06.7	+67 09 17	5.3	10.97	11.37	5.90	0.9430	AGN1	
RX J1828.2+6403	5620	18 28 13.7	+64 03 31	18 28 14.2	+64 03 28	5.2	14.02	14.54	0.06	0.0963	AGN1	
RX J1828.5+6322	5660	18 28 33.0	+63 22 04	18 28 32.2	+63 21 59	4.8	6.85	7.10	...	...	Star	

TABLE 3—*Continued*

Object (1)	NEP Scan No. (2)	α_X (J2000) (3)	δ_X (J2000) (4)	α_{opt} (J2000) (5)	δ_{opt} (J2000) (6)	S/N (7)	$f_{X,det}$ (10^{-14}) (8)	$f_{X,tot}$ (10^{-14}) (9)	L_X (10^{44}) (10)	z (11)	ID (12)	Notes (13)
RX J1828.7+6953	5670	18 28 47.9	+69 53 58	18 28 49.3	+69 54 00	8.2	36.08	37.41	0.21	0.1100	AGN1	
RX J1828.8+6452	5680	18 28 48.6	+64 52 50	18 28 48.3	+64 53 00	6.7	16.26	16.86	7.38	0.8730	AGN1	
RX J1829.0+6433	5690	18 29 00.6	+64 33 49	18 29 00.4	+64 33 51	8.0	22.08	22.89	1.74	0.3880	AGN1	
RX J1829.0+6913	5700	18 29 03.7	+69 13 50	18 29 05.7	+69 14 06	11.5	72.54	96.90	1.77	0.2057	CL	sc = 1.336
RX J1829.3+6409	5710	18 29 19.6	+64 09 18	18 29 17.6	+64 09 17	7.8	13.04	13.52	...	...	Star M	
RX J1829.3+6751	5711	18 29 19.8	+67 51 24	18 29 20.6	+67 51 33	4.2	4.94	5.12	...	...	Star	
RX J1829.5+6905	5730	18 29 32.3	+69 05 09	18 29 31.7	+69 05 13	6.5	12.32	12.78	...	...	Star	
RX J1829.5+6631	5740	18 29 35.4	+66 31 19	18 29 35.4	+66 31 23	4.1	8.57	8.89	2.32	0.6898	AGN1	
RX J1829.7+6749	5750	18 29 43.4	+67 49 09	18 29 42.2	+67 49 12	6.9	20.50	21.26	2.52	0.4783	AGN1	
RX J1829.7+6435	5760	18 29 47.2	+64 35 07	18 29 46.1	+64 35 20	7.6	10.83	11.23	...	...	Star	
RX J1830.0+6645	5790	18 30 01.4	+66 45 23	18 30 02.0	+66 45 23	6.8	18.54	19.22	0.78	0.2889	AGN1	
RX J1830.1+6425	5800	18 30 07.5	+64 25 28	18 30 06.1	+64 25 29	5.5	12.30	12.75	2.70	0.6253	AGN1	
RX J1831.1+6214	5840	18 31 08.6	+62 14 13	18 31 04.5	+62 14 39	8.6	26.73	27.71	...	...	Star	
RX J1831.3+6454	5860	18 31 19.1	+64 54 12	18 31 21.7	+64 54 11	15.7	39.17	40.62	...	...	Star M	
RX J1831.7+6511	5880	18 31 44.4	+65 11 34	18 31 44.4	+65 11 32	10.9	18.10	18.76	...	...	Star	
RX J1832.0+6542	5890	18 32 01.5	+65 42 35	18 32 01.3	+65 42 33	9.2	30.18	31.29	1.29	0.2908	AGN1	
RX J1832.0+7002	5910	18 32 01.8	+70 02 29	18 32 03.9	+70 02 41	9.8	25.72	26.67	...	...	Star	
RX J1832.0+6447	5900	18 32 04.2	+64 47 01	18 32 01.2	+64 47 08	7.1	21.38	22.17	16.75	1.1180	AGN1	
RX J1832.2+6832	5920	18 32 13.3	+68 32 26	18 32 12.3	+68 32 08	4.9	16.06	21.60	0.38	0.1981	CL	sc = 1.345
RX J1832.4+6402	5930	18 32 25.2	+64 02 02	18 32 24.1	+64 02 10	4.8	13.14	13.62	1.00	0.3826	AGN1	
RX J1832.4+6438	5940	18 32 25.2	+64 38 15	18 32 24.2	+64 38 23	6.7	16.87	17.49	2.62	0.5335	AGN1	
RX J1832.5+6836	5950	18 32 31.0	+68 36 50	18 32 29.5	+68 36 52	7.1	16.13	16.73	...	...	Star G5	
RX J1832.5+6449	5960	18 32 31.5	+64 49 49	18 32 32.7	+64 49 59	17.7	95.44	133.99	1.50	0.1610	CL	sc = 1.404
RX J1832.5+6848	5970	18 32 35.0	+68 48 05	18 32 35.6	+68 48 09	20.2	196.34	262.43	4.68	0.2050	CL	sc = 1.337, n
RX J1833.0+6344	5990	18 33 02.8	+63 44 17	18 33 01.3	+63 44 35	5.8	17.23	17.87	2.90	0.5535	AGN1	
RX J1833.5+6431	5992	18 33 30.5	+64 31 46	18 33 29.2	+64 31 54	9.1	16.19	16.79	...	...	Star M	
RX J1833.6+6259	6010	18 33 39.5	+62 59 24	18 33 38.2	+62 59 26	4.7	8.16	8.46	...	...	Star	
RX J1833.7+6521	6020	18 33 44.6	+65 21 37	18 33 43.2	+65 21 39	8.5	25.97	36.40	0.42	0.1621	CL	sc = 1.402
RX J1833.8+6513	6030	18 33 49.1	+65 13 36	18 33 47.8	+65 13 33	4.7	5.00	5.18	...	...	Star	
RX J1834.1+6438	6060	18 34 08.1	+64 38 22	18 34 08.2	+64 38 25	8.0	11.91	12.35	...	...	Star M	
RX J1834.1+7057	6050	18 34 08.2	+70 57 23	18 34 08.5	+70 57 19	9.0	51.12	77.45	0.22	0.0803	CL	sc = 1.515, A 2308, n
RX J1834.5+6931	6051	18 34 33.7	+69 31 37	18 34 33.6	+69 31 45	4.1	6.61	6.85	...	...	Star	
RX J1835.0+6526	6070	18 35 04.8	+65 26 44	18 35 06.0	+65 26 47	7.9	26.12	27.09	2.29	0.4083	AGN1	
RX J1835.1+6342	6080	18 35 08.0	+63 42 33	18 35 10.0	+63 43 14	6.9	28.26	29.31	15.26	0.9445	AGN1	
RX J1835.1+6733	6090	18 35 10.3	+67 33 54	18 35 09.0	+67 33 58	4.4	9.86	10.22	3.17	0.7460	AGN1	
RX J1835.8+6446	6140	18 35 51.0	+64 46 14	18 35 50.7	+64 46 07	5.4	6.13	6.36	...	...	Star M	
RX J1835.9+6336	6150	18 35 55.7	+63 36 57	18 35 53.7	+63 36 53	6.2	10.77	11.17	...	...	Star	
RX J1836.2+6529	6160	18 36 12.0	+65 29 20	18 36 13.5	+65 29 15	4.9	5.89	6.11	...	...	Star F05	HR 7013
RX J1836.3+6654	6163	18 36 22.5	+66 54 47	18 36 22.8	+66 54 54	6.1	7.26	7.53	...	...	Star	
RX J1836.4+6602	6180	18 36 28.2	+66 02 40	18 36 28.7	+66 02 37	5.4	17.34	17.98	0.29	0.1858	AGN1	
RX J1836.5+6344	6190	18 36 31.0	+63 44 30	18 36 30.8	+63 44 39	19.5	145.85	252.72	0.78	0.0846	CL	sc = 1.733
RX J1836.6+6719	6200	18 36 36.1	+67 19 04	18 36 36.8	+67 19 12	4.7	11.52	11.94	0.42	0.2693	AGN1	
RX J1836.9+6747	6210	18 36 54.7	+67 47 12	18 36 55.7	+67 47 09	5.5	7.50	7.78	...	...	Star	
RX J1837.5+6231	6240	18 37 34.0	+62 31 23	18 37 33.6	+62 31 31	5.3	9.41	9.75	...	...	Star A0 V	HR 7018
RX J1838.1+6649	6280	18 38 09.1	+66 49 26	18 38 10.0	+66 49 22	4.4	11.10	11.51	0.46	0.2879	AGN1	
RX J1838.2+6321	6290	18 38 12.6	+63 21 02	18 38 14.6	+63 21 21	8.4	31.52	41.73	0.86	0.2167	CL	sc = 1.324
RX J1838.8+6432	6300	18 38 51.9	+64 32 21	18 38 53.1	+64 32 23	4.3	10.24	10.61	1.21	0.4700	AGN1	

TABLE 3—*Continued*

Object (1)	NEP Scan No. (2)	α_X (J2000) (3)	δ_X (J2000) (4)	α_{opt} (J2000) (5)	δ_{opt} (J2000) (6)	S/N (7)	$f_{X, det}$ (10^{-14}) (8)	$f_{X, tot}$ (10^{-14}) (9)	L_X (10^{44}) (10)	z (11)	ID (12)	Notes (13)
RX J1839.2+6711	6301	18 39 16.9	+67 11 12	18 39 16.5	+67 11 06	4.2	8.69	9.01	2.53	0.7130	AGN1	
RX J1839.2+7018	6330	18 39 17.4	+70 18 20	18 39 17.2	+70 18 24	4.1	12.37	16.22	0.38	0.2297	CL	sc = 1.312
RX J1839.3+6544	6340	18 39 18.5	+65 44 42	18 39 18.3	+65 44 35	4.1	12.15	12.60	0.04	0.0820	AGN1	
RX J1839.4+6903	6350	18 39 25.6	+69 03 06	18 39 25.4	+69 02 54	11.7	45.90	47.59	...	...	Star	
RX J1839.8+6537	6370	18 39 48.6	+65 37 57	18 39 47.5	+65 37 59	8.3	17.32	17.96	...	...	Star	
RX J1840.5+6521	6390	18 40 34.2	+65 21 29	18 40 33.6	+65 21 37	6.0	9.29	9.63	...	...	Star M	
RX J1840.7+7038	6400	18 40 43.1	+70 38 40	18 40 44.4	+70 38 47	5.3	10.48	10.86	...	...	Star	
RX J1840.9+6245	6410	18 40 54.6	+62 45 00	18 40 56.6	+62 44 54	10.7	31.25	32.41	...	...	Star K0 III	HR 7042
RX J1840.9+6528	6420	18 40 58.1	+65 28 36	18 40 58.6	+65 28 34	5.6	9.05	9.38	...	...	Star	
RX J1841.3+6321	6450	18 41 18.9	+63 21 36	18 41 20.0	+63 21 42	4.4	12.08	12.53	18.18	1.4990	AGN1	
RX J1841.9+6316	6451	18 41 59.4	+63 16 29	18 41 57.8	+63 16 26	12.4	34.05	35.31	...	...	Star M	
RX J1842.2+6204	6452	18 42 14.8	+62 04 24	18 42 15.6	+62 04 24	4.6	18.33	19.01	0.96	0.3203	AGN1	
RX J1842.5+6809	6490	18 42 33.0	+68 09 30	18 42 33.3	+68 09 25	11.6	66.66	69.12	8.07	0.4750	AGN1	n
RX J1842.9+6241	6491	18 42 56.4	+62 41 44	18 42 55.2	+62 41 49	10.5	63.19	65.52	0.20	0.0835	AGN1	
RX J1843.2+6956	6510	18 43 16.3	+69 56 03	18 43 12.6	+69 55 54	6.1	17.86	18.52	...	...	Star	
RX J1843.3+6653	6520	18 43 22.5	+66 53 21	18 43 20.9	+66 53 29	5.0	14.79	15.33	0.81	0.3273	AGN1	
RX J1843.7+6514	6530	18 43 47.9	+65 14 03	18 43 46.0	+65 14 08	7.1	13.04	13.52	...	...	Star	
RX J1843.9+6821	6540	18 43 55.7	+68 21 11	18 43 54.1	+68 21 01	6.2	25.86	26.81	1.82	0.3688	AGN1	
RX J1844.2+6719	6541	18 44 13.8	+67 19 42	18 44 14.6	+67 19 33	6.6	9.41	9.75	...	...	Star M	
RX J1844.3+6431	6542	18 44 23.4	+64 31 31	18 44 21.8	+64 31 46	4.8	13.54	14.04	1.73	0.4870	AGN1	
RX J1844.4+6236	6543	18 44 26.9	+62 36 12	18 44 26.4	+62 36 14	7.0	34.49	35.76	1.77	0.3172	AGN1	
RX J1844.4+6248	6544	18 44 27.5	+62 48 27	18 44 26.2	+62 48 29	7.0	30.09	31.20	75.12	1.8800	AGN1	
RX J1844.6+6338	6545	18 44 40.0	+63 38 27	18 44 39.1	+63 38 28	6.2	10.00	10.37	...	...	Star	
RX J1844.9+6813	6570	18 44 54.0	+68 13 23	18 44 54.1	+68 13 17	6.9	32.06	33.25	1.56	0.3097	AGN1	

Note.—Table 3 is also available in machine-readable form in the electronic edition of the *Astrophysical Journal*.

flux using conversion factors based on three different types of source spectra (see § 2).

Column (9).—Total unabsorbed flux in the 0.5–2.0 keV band ($f_{\rm X,tot}$, 10^{-14} ergs cm^{-2} s^{-1}). The total flux accounts for the flux outside the photometry aperture and reflects the size correction applied to the detect flux. For point sources this flux correction factor is constant and equal to 1.0369 (see § 2), while it varies for extended sources, such as clusters or groups of galaxies. The flux correction factor for extended sources is given in column (13).

Column (10).—Rest-frame *K*-corrected luminosities in the 0.5–2.0 keV band ($L_{\rm X}$, 10^{44} ergs s^{-1}) for extragalactic objects with uncertainties based on the fractional errors on the source count rate. *K*-correction factors for clusters of galaxies, assuming a Raymond-Smith plasma spectrum with a metallicity 0.3 solar, are 0.76, 0.95, and 1.01, minimum, median, and maximum values, respectively. For AGNs the assumed power-law spectrum with energy index $=-1$ gives a formal *K*-correction factor of 1.

Column (11).—Spectroscopically measured redshift for all extragalactic sources. Typical uncertainty is $\leq$0.001.

Column (12).—Optical identification of the X-ray source: AGN for active galactic nucleus, either type 1 (AGN1) or type 2 (AGN2) (see § 4); STAR for star; CL for group or cluster of galaxies; BL for BL Lacertae object; GAL for normal galaxy and PN for Planetary Nebula. Spectral type for stars is also indicated if known.

Column (13).—Comments regarding the source, such as size correction factor (sc = size$_{\rm corr}$) for galaxy clusters, or indication of a note (n) to the source given in § 6.

6. NOTES TO INDIVIDUAL SOURCES

RX J1716.2+6836.—Also called RX J1716.0+6836 in Boller et al. (1997). The identification comes from the revised Burbidge catalog (Hewitt & Burbidge 1993).

RX J1717.7+6431.—There is a star within the error circle that is closer to the X-ray position (7$''$.7) than the AGN2. We still believe that the AGN2 is the correct identification, not only because it is an AGN but also because it appears to be in a distorted spiral in our UH 2.2 m *B*-band image. Distortion implies some kind of interaction and often these distorted galaxies are X-ray sources.

RX J1719.8+6457.—This source is one of two sources in the NEP still unidentified. Optical spectra were taken for seven objects within 80$''$ from the X-ray position, but no plausible identification was found.

RX J1720.8+6210.—There are two galaxies at the same redshift as the AGN1 ($z=0.7313$) and closer to the X-ray centroid (approximate positions from DSS-2 red are for cfh 11, $\alpha_{2000}=17^{\rm h}20^{\rm m}46^{\rm s}.8$, $\delta_{2000}=+62°10'25''$; and for cfh 12b, $\alpha_{2000}=17^{\rm h}20^{\rm m}43^{\rm s}.9$, $\delta_{2000}=+62°10'11''$). We still identify the source as AGN1 since its spectrum shows a broad Mg II emission line (FWHM $>$ 4000 km s^{-1}). However, the presence of a distant cluster at $z\sim0.73$ is not excluded.

RX J1723.1+6826.—This source is identified with a QSO ($\alpha_{2000}=17^{\rm h}23^{\rm m}09^{\rm s}.9$, $\delta_{2000}=+68°26'56''$, $z=0.9782\pm0.001$) that is 4$''$ away from the X-ray centroid. The optical spcetrum shows a very broad Mg II emission line (FWHM $\geq$ 7000 km s^{-1}). A second object at $\alpha_{2000}=17^{\rm h}23^{\rm m}10^{\rm s}.1$, $\delta_{2000}=+68°26'51''$, just south of the QSO and only 3$''$.4 away from the X-ray centroid, has a similar redshift ($z=0.9777$) as the QSO. This second object is fainter and has a narrower Mg II line in emission. Both objects could contribute to the X-ray emission even if we indicate the object with broader Mg II line as the identification in the table.

RX J1724.1+7000 and RX J1724.2+6956.—These two sources were identified as a group of galaxies in Henry et al. (1995). The X-ray morphology is complex and elongated along the north-south direction (see Fig. 1*a* in Henry et al. 1995). We confirm here the identification of these sources with a single group of galaxies at $z=0.0386$.

RX J1727.0+6926.—A radio source (0.96 $\pm$ 0.06 mJy at 6 cm) was detected with the VLA in the DnC array at the position of the optical counterpart by T. Rector (2003, private communication).

RX J1727.8+6748.—There are several galaxies in the area for which no optical spectrum is available. The suggested identification is the AGN1 at $z=0.4950$ ($\alpha_{2000}=17^{\rm h}27^{\rm m}45^{\rm s}.5$, $\delta_{2000}=+67°48'43''$) lying 22$''$ away from the X-ray centroid, with a broad (FWHM $>$ 7000 km s^{-1}) Mg II emission line in its optical spectrum.

RX J1732.5+7031.—This object appears in the sample of identified northern *ROSAT* sources by Appenzeller et al. (1998) with a redshift $z=0.209$ versus our $z=0.2114$.

RX J1732.9+6533.—The redshift for this QSO ($z=0.8560$) comes from Hewitt & Burbidge (1993).

RX J1736.3+6802.—This group of galaxies was published in Henry et al. (1995). There are 12 galaxies with spectroscopic redshifts. Refer to Henry et al. (1995) for more details and for an X-ray contour image (their Fig. 1*c*).

RX J1736.9+6845.—This X-ray source is MS 1737.2+6847 and its identification with SAO17576 (Ω Draconis) comes from the EMSS; see Stocke et al. (1991) and Maccacaro et al. (1994).

RX J1736.4+6828.—The X-ray source is identified with GAT 732, a star with an *E* magnitude in APM of 8.98. The star has a high proper motion (about 1$'$ in 50 yr).

RX J1739.7+6710.—This source is MS 1739.8+6712 and is identified as AGN1. The redshift, $z=0.118$, comes from Stocke et al. (1991); an optical finding chart is published in Maccacaro et al. (1994).

RX J1741.2+6507.—There is a cluster candidate in the field of this source identified as AGN1 at $z=0.7466$. We have concordant redshifts for two galaxies (A and B): $\alpha_{2000}=17^{\rm h}41^{\rm m}15^{\rm s}.5$, $\delta_{2000}=+65°07'53''$, $z_A=0.3797$; $\alpha_{2000}=17^{\rm h}41^{\rm m}07^{\rm s}.7$, $\delta_{2000}=+65°07'47''$, $z_B=0.3775$.

RX J1743.4+6341.—This cluster, associated with A2280, has a large gravitational arc that is described in Gioia et al. (1995).

RX J1745.2+6556.—In the field of this source, identified as a cluster of galaxies at $z=0.6080\pm0.0005$ (optical spectrum for a member galaxy is shown in Fig. 10) there is also an AGN ($\alpha_{2000}=17^{\rm h}45^{\rm m}17^{\rm s}.6$, $\delta_{2000}=+65°56'02''$, $z=0.2904$) that is $\sim$18$''$ away from the X-ray centroid. The AGN could contribute to the X-ray emission of the source. However, it is difficult to classify the AGN as type 1 or type 2 since there is no Hβ emission line, and the Hα emission line is blended with N II. The spectrum of the AGN has a very red continuum.

RX J1746.1+6737.—The identification of this X-ray source comes from the EMSS. This is MS 1746.2+6738 identified as AGN1 at $z=0.041$ by Stocke et al. (1991). The AGN1 ($\alpha_{2000}=17^{\rm h}46^{\rm m}08^{\rm s}.8$, $\delta_{2000}=+67°37'15''$) is 25$''$ south of a bright SAO star (SAO17632, $\alpha_{2000}=17^{\rm h}46^{\rm m}08^{\rm s}.7$,

$\delta_{2000} = +67°37'43''$, $m_V = 7.79$), which could also contribute to the X-ray emission.

RX J1746.2+6227.—The redshift for this QSO ($z = 3.889$) is taken from Hook et al. (1995; see their Fig. 2 for a spectrum). Stickel (1993) gives a redshift of $z = 3.886$ for this object. The QSO was independently discovered as an X-ray source by Becker, Helfand, & White (1992), who measured a redshift of $z = 3.87$ (optical spectrum in their Fig. 2). An X-ray spectrum with *ASCA* is published in Figure 1 of Kubo et al. (1997).

RX J1747.0+6836.—This very bright source is MS 1747.2+6837. The identification as AGN1 ($z = 0.063$) comes from Kriss & Canizares (1982) and Stocke et al. (1991). P. F. Winkler (1982, private communication) originally discovered this object.

RX J1747.4+6626.—There are two objects here, both AGN1 and at the same redshift ($z = 0.1391$), which could both contribute to the X-ray emission. The optical position for one of them is $\alpha_{2000} = 17^h27^m47\overset{s}{.}0$, $\delta_{2000} = +66°26'24''$ (given in Table 3). The second object, which is a spiral galaxy at $z = 0.1390$, is at $\alpha_{2000} = 17^h47^m26\overset{s}{.}6$, $\delta_{2000} = +66°26'05''$.

RX J1747.9+6623.—We identify this source as a normal galaxy (GAL), but there are two objects possibly interacting. Object A ($\alpha_{2000} = 17^h47^m58\overset{s}{.}5$, $\delta_{2000} = +66°23'26''$, $z = 0.1739$) is a narrow emission-line galaxy with Hα, Hβ, Hγ, and [O III] emission lines in the optical spectrum and shows the morphology of a disturbed spiral. Object B ($\alpha_{2000} = 17^h47^m56\overset{s}{.}8$, $\delta_{2000} = +66°23'46''$, $z = 0.1737$) does not show any emission line in the spectrum and resembles an edge-on spiral in our UH 2.2 m open image.

RX J1748.5+7005.—Identification and redshift for this BL Lac comes from the literature. An optical spectrum is published in Figure 7 of Lawrence et al. (1996); see also note in Rector & Stocke (2001).

RX J1748.6+6842.—There are two AGNs with similar redshift ($z = 0.0537$ and $z = 0.0540$) that are blended in the APM finder. The western object ($\alpha_{2000} = 17^h48^m38\overset{s}{.}3$, $\delta_{2000} = +68°42'17''$) has broad emission lines in its optical spectrum. We indicate this object as the identification (AGN1). The eastern object ($\alpha_{2000} = 17^h48^m38\overset{s}{.}7$, $\delta_{2000} = +68°42'16''$) has H$\alpha$ in emission but it is difficult to assess the width of the emission line since the spectrum is rather noisy. Both objects look like spiral galaxies in our UH 2.2 m open image. The two objects might be interacting, and both could contribute to the X-ray emission.

RX J1751.2+6533.—This source is associated with the group of galaxies published in Figure 1*e* of Henry et al. (1995). The redshift has been updated using more accurate low-redshift data from Falco et al. (1999).

RX J1751.5+7013.—This source is identified with a cluster of galaxies at $z = 0.4925$. The two galaxies, for which we have optical spectra, have narrow emission lines typical of AGN2. One of the AGN2 ($\alpha_{2000} = 17^h52^m33\overset{s}{.}1$, $\delta_{2000} = +70°13'01''$, $z = 0.4936$) has a narrow Mg II line in emission, in addition to Hβ and to [O II] and [O III] lines.

RX J1752.2+6522.—This source is identified as a cluster of galaxies at $z = 0.3923$. There is also an emission-line object ($\alpha_{2000} = 17^h52^m12\overset{s}{.}9$, $\delta_{2000} = +65°22'36''$) that is $15\overset{''}{.}1$ away from the X-ray position with $z = 0.3940$. We still identify the source with a cluster of galaxies since the spectrum of the AGN, with Hβ in emission, is too noisy to assess the width of the line.

RX J1753.9+7016.—This source is MS 1754.5+7017 and is identified as an AGN1 at $z = 0.062$ by Stocke et al. (1991).

RX J1754.0+6452.—The redshift for this cluster is tentative because it is based on three low S/N spectra.

RX J1754.6+6803.—This is MS 1754.9+6803. The redshift ($z = 0.0770$) was measured by Stocke et al. (1991) and is based on three galaxy spectra taken at the MMT in 1985 April.

RX J1756.2+7042.—This is one of the two still unidentified sources in the whole NEP survey. The X-ray source is a double source elongated in the east-west direction. The eastern X-ray centroid is identified with an AGN1 ($\alpha_{2000} = 17^h56^m14\overset{s}{.}9$, $\delta_{2000} = +70°41'56''$, $z = 0.838$) since it shows a broad Mg II line in emission in its optical spectrum. The western source is still unidentified. We have taken spectra for several objects in the area using the Keck II, but none of the objects seems to be a satisfactory identification.

RX J1757.2+7033.—This source is MS 1757.7+7034, identified by Stocke et al. (1991) as a BL Lac at $z = 0.407$, from Ca II H and K, *G* band, and Mg I *b* absorption lines.

RX J1757.2+6547.—This X-ray source, identified with an M star ($\alpha_{2000} = 17^h57^m14\overset{s}{.}3$, $\delta_{2000} = +65°46'58''$, $m_E = 14.68$), is $9\overset{''}{.}4$ away from the X-ray centroid in the APM finders. There is also an AGN1 ($\alpha_{2000} = 17^h57^m13\overset{s}{.}6$, $\delta_{2000} = +65°46'45''$, $z = 0.578$) $15\overset{''}{.}7$ away from the X-ray centroid with $m_E = 19.53$ and $m_O = 20.0$. The AGN1 could also contribute to the X-ray emission of the source.

RX J1757.3+6631.—There are five spectroscopic redshifts for this cluster at $z = 0.6909$. The spectra were taken at the CFHT. None of the five galaxies are visible on the APM, thus the optical positions are approximate coordinates measured from the DSS-2 red plate. Two of the cluster galaxies (cfh 2 at $\alpha_{2000} = 17^h57^m46\overset{s}{.}3$, $\delta_{2000} = +66°30'26''$, $z = 0.7006$; and cfh 8 at $\alpha_{2000} = 17^h57^m29\overset{s}{.}9$, $\delta_{2000} = +66°32'29''$, $z = 0.6860$) are identified as AGN2 galaxies since their optical spectra show similar narrow forbidden [O III], [O II] and permitted Hβ and Hγ emission lines.

RX J1757.9+6609.—This source is identified with an AGN2 ($\alpha_{2000} = 17^h57^m56\overset{s}{.}5$, $\delta_{2000} = +66°09'20''$, $z = 0.4865$) only 4'' away from the X-ray position. See Figure 6 for an optical spectrum of the AGN2. However, spectroscopic redshifts for two galaxies ($\alpha_{2000} = 17^h58^m02\overset{s}{.}1$, $\delta_{2000} = +66°09'34''$, and $\alpha_{2000} = 17^h58^m00\overset{s}{.}6$, $\delta_{2000} = +66°07'35''$) that are located 36'' and 106'' away from the X-ray centroid, respectively, are concordant with the redshift of NEP super cluster ($z = 0.089$) found in the NEP survey by Mullis et al. (2001).

RX J1758.9+6520.—This source is identified with a cluster of galaxies at $z = 0.3652$. Three cluster galaxies spectroscopically observed have narrow emission lines (see Fig. 7 for an example of one cluster member, namely, galaxy C at $\alpha_{2000} = 17^h58^m53\overset{s}{.}8$, $\delta_{2000} = +65°21'02''$, $z_C = 0.3665$). A fourth object in the field at $\alpha_{2000} = 17^h59^m02\overset{s}{.}8$, $\delta_{2000} = +65°20'55''$, has broad emission lines and is thus identified as AGN1 ($z = 0.3660$). The identification of the source is still a cluster of galaxies based on the distance of the AGN1 from the X-ray position ($\sim$35''), but a contribution to the X-ray emission from the AGN1 is not excluded. Thus, this source is a case of cluster plus AGN.

RX J1759.7+6629.—This X-ray source (AGN1 at $z = 0.399$) was already identified by Bower et al. (1996). We took an additional spectrum to confirm the QSO nature.

RX J1800.0+6645.—This X-ray source is the same as RX J1800.0+6646 in Bower et al. (1996) and was identified as a G type star. Our spectrum confirms that the object is a G-K type star.

RX J1800.1+6636.—This X-ray source was already identified by Bower et al. (1996) as a Sy2 galaxy (NGC 6552). We took an additional spectrum ($z = 0.0260$) to confirm the AGN2 nature.

RX J1801.2+6902.—The redshift for this source (AGN1, $z = 1.27$) comes from Lacy et al. (1993).

RX J1801.2+6624.—This X-ray source was already identified in Bower et al. (1996) as a QSO at $z = 1.25$.

RX J1801.7+6638.—This is a bright X-ray source identified as a BL Lac in Bower et al. (1996; see finding chart in their Fig. 2*c* and an optical spectrum in their Fig. 6). The redshift is unknown since the optical spectrum is featureless. A radio source (1.07 ± 0.04 mJy at 6 cm) was detected with the VLA in the DnC array at the position of the optical source by T. Rector (2003, private communication).

RX J1802.0+6629.—This source was identified as a BL Lac in Bower et al. (1996) given the very weak or almost absent lines in the spectrum they obtained at the Multiple Mirror Telescope (see their Fig. 3). An optical spectrum of this same source was obtained by us in 1999 July with KeckII-LRIS (see Fig. 12). Strong and broad Balmer emission lines are visible in our spectrum consistent with an AGN1 object, possibly a variable QSO?

RX J1802.7+6727.—This source is identified as an AGN2 at $z = 0.1620$. There are two possibly interacting spiral galaxies with optical narrow emission lines in their spectra, which are blended on the APM finder. The optical position of galaxy A1, at ($z = 0.1605$), is $\alpha_{2000} = 18^h02^m47^s.8$, $\delta_{2000} = +67°27'41''$, while the optical position of galaxy A2, at $z = 0.1635$, is $\alpha_{2000} = 18^h02^m47^s.6$, $\delta_{2000} = +67°27'34''$. Both galaxies could be responsible for part of the X-ray emission.

RX J1803.4+6738.—This very bright NEP source is MS 1803+6728 and is identified as AGN1. The redshift ($z = 0.1360$) was measured by Stocke et al. (1991). The object is also listed in the QSO catalog by Hewitt & Burbidge (1993) as HB89, and in the X-ray NORAS catalog by Böhringer et al. (2000) as a tentative AGN. Optical spectra taken at Lick and Multiple Mirror Telescope observatories are shown in Figure 4 of Treves et al. (1995).

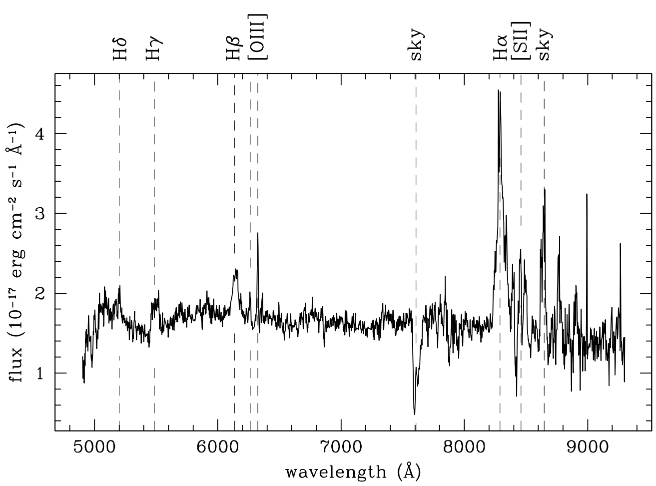

FIG. 12.—RX J1802.0+6629: AGN1 at $z = 0.2650 \pm 0.001$. Long-slit spectrum of the AGN1 ($\alpha_{2000} = 18^h02^m04^s.8$, $\delta_{2000} = +66°29'14''$) obtained with Keck II LRIS on 1999 July 21. The total integration time was 30 minutes. The dashed lines indicate the positions of the emission lines at the redshift of the AGN1. Wavelengths of atmospheric absorption bands are also indicated. This X-ray source was identified as a BL Lac by Bower et al. (1996). Either the BL Lac was in a quiescent state or the object identified by Bower et al. (1996) is a different object.

RX J1803.9+6548.—The redshift for this BL Lac ($z = 0.0850$) is tentative since it has been derived from very weak absorption lines. The source is also identified with the VLA radio source NEP J1803.9+6548 by Kollgaard et al. (1994), and it is in the radio-loud *ROSAT* NEP sources detected with the VLA at 1.5 Ghz by Brinkmann et al. (1999) with a flux $=43.1 \pm 1.7$ mJy (see more references therein).

RX J1804.3+6629.—This source is identified with a very hot, subdwarf star. Its optical position, $\alpha_{2000} = 18^h04^m24^s.7$, $^s.7$, $\delta_{2000} = +66°29'28''$, is 26″ away from the X-ray position. There is a second object in the field that is closer ($\alpha_{2000} = 18^h04^m20^s.6$, $\delta_{2000} = +66°29'54''$) to the center of the X-ray emission and for which no spectrum is available. However, this second object is quite faint, is not blue on the DSS, does not have any radio emission, and thus is unlikely to be an AGN.

RX J1806.1+6813.—This source is identified as cluster of galaxies at $z = 0.303$. Four out of six galaxies for which we have taken spectra are emission-line galaxies, all with concordant redshifts. One of the four galaxies ($\alpha_{2000} = 18^h06^m04^s.8$, $\delta_{2000} = +68°13'08''$, $z = 0.2953$) has broad Balmer (FWHM = 2500 km s^{-1}). Thus, this source is a case of cluster plus AGN.

RX J1806.4+7028.—This source is identified as a galaxy and has an X-ray luminosity $L_X = 1.8 \times 10^{43}$ ergs s^{-1} (assuming $kT = 2$ keV), which is high for a galaxy with no emission lines. As first noted by Mullis (2001) it could be an example of overluminous galaxies found in X-ray surveys (e.g., Vikhlinin et al. 1999 and references therein).

RX J1806.8+6949.—This is a BL Lac in a cluster of galaxies. Redshift comes from Falco et al. (1999).

RX J1808.8+6634.—The redshift for this source, identified as AGN1 at $z = 0.697$, comes from Laurent-Muehleisen et al. (1998). See their Table 2 for source properties.

RX J1810.3+6328.—This source, identified as AGN1 at $z = 0.838$, has a double morphology in X-rays. The identification of the X-ray source given in Table 3 refers to the western lobe ($\alpha_{2000} = 18^h10^m31^s.1$, $\delta_{2000} = +63°28'08''$, $z = 0.838$). The eastern lobe is an AGN1 at $z = 1.0907$ ($\alpha_{2000} = 18^h10^m16^s.9$, $\delta_{2000} = +63°29'14''$).

RX J1815.4+6806.—The redshift for this QSO ($z = 0.239$) comes from Lacy et al. (1993).

RX J1821.9+6420.—The identification of this source as a QSO at $z = 0.2970$ comes from Pravdo & Marshall (1984; see an optical spectrum in their Fig. 2). However, as already noted by Hutchings & Neff (1991, see their Fig. 1), a cluster of galaxies for which six galaxy spectra were taken by Schneider et al. (1992) is present at the same redshift as the QSO (see detailed description of this QSO/cluster source in Wold et al. 2002 and references therein). The X-ray source has the highest S/N of the whole NEP survey, it is extremely X-ray luminous ($L_X = 5.61 \times 10^{45}$ ergs s^{-1}), and it is also an *IRAS* source, as reported by de Grijp et al. (1992).

RX J1826.6+6706.—This source is identified with an AGN1 at $z = 0.287$. The redshift comes from Lacy et al. (1993).

RX J1832.5+6848.—This source is identified as a cluster of galaxies at $z = 0.205$. We took optical spectra for three galaxies and they have concordant redshifts. The source is listed in the literature as the radio source 7C 1832+6845, and it is identified as QSO by Veron-Cetty & Veron (2001), and as BL Lac in the NORAS catalog by Böhringer et al. (2000). The ambiguity may be due to the fact that there are two distinct objects very closely separated ($\sim 6''$) at the position of the X-ray source. The northwest object, object A, is the object we have observed spectroscopically ($\alpha_{2000} = 18^{h}32^{m}35\overset{s}{.}6$, $\delta_{2000} = +68°48'09''$, $z = 0.2049$). It is red on the DSS, and its spectrum shows narrow Balmer and oxygen emission lines, consistent with an AGN2 object (unless we caught the QSO in a quiescent state). The southeast object A1 ($\alpha_{2000} = 18^{h}32^{m}36\overset{s}{.}2$, $\delta_{2000} = +68°48'04''$) appears blue on the DSS and could be the object indicated as QSO or BL Lac in the literature. No spectrum is available for A1. A second galaxy in the cluster (object B at $\alpha_{2000} = 18^{h}32^{m}35\overset{s}{.}9$, $\delta_{2000} = +68°47'43''$, $z = 0.2048$) also shows narrow emission lines and it is classified as AGN2 in the cluster. The third galaxy for which we obtained a spectrum, object C ($\alpha_{2000} = 18^{h}32^{m}35\overset{s}{.}6$, $\delta_{2000} = +68°47'58''$, $z = 0.2054$), shows no emission lines in its spectrum.

RX J1834.1+7057.—This source is very extended in X-rays, and it is identified with a cluster of galaxies at $z = 0.0803$. An extraction radius of $6\overset{'}{.}5$ has been used, different from the normal $5'$ radius used for the rest of the X-ray sources. The X-ray position is centered on a bright galaxy ($\alpha_{2000} = 18^{h}34^{m}08\overset{s}{.}5$, $\delta_{2000} = +70°57'19''$, $m_E =\sim 12.5$), possibly the cD, whose redshift appears in the NORAS catalog of Böhringer et al. (2000) as $z = 0.0824$. The source is in the same region of sky as A2308, even if the Abell cluster position in the NED database is at $\alpha_{2000} = 18^{h}33^{m}33\overset{s}{.}8$ and $\delta_{2000} = +71°01'28''$. The redshift given in Table 3 has been computed using spectra for three galaxies taken by us at the UH 2.2 m. The redshift agrees with other redshift determinations listed in NED for A2308.

RX J1842.5+6809.—Redshift for this AGN1, $z = 0.4750$, comes from the literature. The QSO is listed in the catalog by Hewitt & Burbidge (1993) and in Xu et al. (1994).

7. SUMMARY

We have presented data for a survey performed at X-ray wavelengths using the RASS data in a 80.7 deg^2 contiguous area of sky at the North Ecliptic Pole. The NEP survey is centered at $\alpha_{2000} = 18^{h}00^{m}$, $\delta_{2000} = +66°33'$ and is at a moderate Galactic latitude of $b = 29\overset{\circ}{.}8$. The NEP catalog consists of a homogeneous, flux-limited sample of 445 individual X-ray sources above a flux of $\sim 2 \times 10^{-14}$ ergs cm^{-2} s^{-1} in the 0.5–2.0 keV energy band. The main results of this paper are the optical identifications of the X-ray sources of the NEP survey. Basic X-ray and optical properties of the sources are presented here, while finding charts for all the sources with overlayed X-ray contours will be made available in a separate publication (see also Appendix C in Mullis 2001). We have described in detail the optical identification procedure. We have identified 443 out of 445 X-ray sources (99.6%) and determined spectroscopic redshifts for the extragalactic objects. All the NEP sources are identified with previously known classes of X-ray emitters. The optical content of the survey can be summarized as follows: 218 AGNs (49.4%), 152 stars (34.3%), 62 clusters of galaxies (14.0%), eight BL Lacertae objects (1.8%), one individual galaxy (0.2%), and one planetary nebula (0.2%). Given the completeness of the optical identification and the well-defined selection criteria, the NEP survey can be used to characterize the evolutionary properties of the extragalactic populations. Evidence for cluster X-ray luminosity negative evolution using the NEP clusters has already appeared in Gioia et al. (2001), while the X-ray evolutionary properties of the NEP AGNs will be the subject of future publications.

I. M. G. notes that this paper was written in spite of the continued efforts by the Italian government to dismantle publicly funded fundamental research. We are grateful to the University of Hawai'i Telescope Allocation Committee for its generous support of this program. The staffs of the University of Hawai'i, Canada-France-Hawai'i, Keck, Multiple Mirror Telescope and F. L. Whipple Observatory telescopes performed with their customary expertise. Many thanks are also due to the *ROSAT* team, particularly Günther Hasinger and Joachim Trümper. We would like to thank Travis Rector at NRAO for observing with the Very Large Array two NEP sources whose radio detection confirmed their BL Lac nature. We are grateful to the sponsoring agencies who have enabled this project. Support has come from the NSF (AST 91-19216 and AST 95-00515), NASA (NGT5-50175, GO-5402.01-93A, and GO-05987.02-94A), the ARCS Foundation, the Smithsonian Institution, NATO (CRG91-0415), the Italian Space Agency ASI-CNR, the Bundesministerium für Forschung (BMBF/DLR), and the Max-Planck-Gesellschaft (MPG). This research has made use of the NASA/IPAC Extragalactic database (NED), which is operated by the Jet Propulsion Laboratory, California Institute of Technology, under contract with the National Aeronautics and Space Administration.

REFERENCES

Appenzeller, I., et al. 1998, ApJS, 117, 319
Aussel, H., Coia, D. Mazzei, P. De Zotti, G., & Franceschini, A. 2000, A&AS, 141, 257
Becker, R. H., Helfand, D. J., & White, R. L. 1992, AJ, 104, 531
Bennet, C. L., et al. 1996, ApJ, 464, L1
Boese, F. G. 2000, A&AS, 141, 507
Böhringer, H., et al. 2000, ApJS, 129, 435
———. 2001, A&A, 369, 826
Boller, T., Brandt, W. N., Fabian, A. C., & Fink, H. H. 1997, MNRAS, 289, 303
Bower, R. G., et al. 1996, MNRAS, 281, 59
Boyle, B. J., Shanks, T., & Peterson, B. A. 1988, MNRAS, 235, 935
Brinkmann, W. Chester, M., Kollgaard, R., Feigelson, E., Voges, W., & Hertz, P. 1999, A&AS, 134, 221
Burke, D. J., Collins, C. A., Sharples, R. M., Romer, A. K., Holden, B. P., & Nichol, R. C. 1997, ApJ, 488, L83
Campana, S., Lazzati, D., Panzera, M. R., & Taglaferri, G. 1999, ApJ, 524, 423
Castander, F. J., et al. 1995, Nature, 377, 39
Cavaliere, A., & Fusco-Femiano, R. 1976, A&A, 49, 137
Christian, C. A., Adams, M., Barnes, J. V., Hayes, D. S., Siegel, M., Butcher, H., & Mould, J. R. 1985, PASP, 97, 363
Collins, C. A., et al. 1997, ApJ, 479, L117
De Grandi, S., et al. 1999, ApJ, 514, 148
de Grijp, M. H. K., Keel, W. C., Miley, G. K., Goudfrooij, P., & Lub, J. 1992, A&AS, 96, 389
Donahue, M., et al. 2002, ApJ, 569, 689
Ebeling, H., Edge, A. C., Allen, S. W., Crawford, C. S., Fabian, A. C., & Huchra, J. P. 2000, MNRAS, 318, 333
Ebeling, H., Edge, A. C., Böhringer, H., Allen, S. W., Crawford, C. S., Fabian, A. C., Voges, W., & Huchra, J. P. 1998, MNRAS, 301, 881
Ebeling, H., Edge, A. C., & Henry, J. P. 2001, ApJ, 553, 668

Elvis, M., Lockmann, F. J., & Fassnacht, C. 1994, ApJS, 95, 413
Falco, E. E., et al. 1999, PASP, 111, 438
Foltz, C., & Smith, D. 1994, The MMT Spectrograph Operation Manual
Gaidos, E. J., Magnier, E. A., & Schechter, P. L. 1993, PASP, 105, 1294
Gioia, I. M., Henry, J. P., Maccacaro, T., Morris, S. L., Stocke, J. T., & Wolter, A. 1990a, ApJ, 356, L35
Gioia, I. M., Henry, J. P., Mullis, C. R., Voges, W., Briel, U. G., Böhringer, H., & Huchra, J. P. 2001, ApJ, 553, L105
Gioia, I. M., Maccacaro, T., Schild, R. E., Wolter, A., Stocke, J. T., Morris, S. L., & Henry, J. P. 1990b, ApJS, 72, 567
Gioia, I. M., et al. 1995, A&A, 297, L75
Hacking, P., & Houck, J. R. 1987, ApJS, 63, 311
Heasley, J. N., & Christian, C. A. 1986, ApJ, 307, 738
Henry, J. P., Gioia, I. M., Maccacaro, T., Morris, S. M., Stocke, J. S., & Wolter, A. 1992, ApJ, 386, 408
Henry, J. P., Gioia, I. M., Mullis, C. R., Voges, W., Briel, U. G., Böhringer, H., & Huchra, J. P. 2001, ApJ, 553, L109
Henry, J. P., et al. 1995, ApJ, 449, 442
Hewitt, A., & Burbidge, G. 1993, ApJS, 87, 451
Hook, I. M., McMahon, R. G., Irwin, M. J., & Hazard, C. 1996, MNRAS, 282, 1274
Hook, I. M., McMahon, R. G., Patnaik, A. R., Browne, I. W. A., Wilkinson, P. N., Irwin, M. J., & Hazard, C. 1995, MNRAS, 273, L63
Hutchings, J. B., & Neff, S. G. 1991, AJ, 101, 2001
Kollgaard, R. I., Brinkmann, W., Chester, M. M., Feigelson, E. D., Hertz, P. Reich, P., & Wielebinski, R. 1994, ApJS, 93, 145
Kreysing, H. C., Diesch, C., Zweigle, J., Staubert, R., Grewing, M., & Hasinger, G. 1992, A&A, 264, 623
Kriss, G., & Canizares, C. 1982, ApJ, 261, 51
Kubo, H., Makishima, K., Takahashi, T., Ishida, M., Inoue, H., Matsuoka, M., Yamasaki, N., & Suzuki, K. 1997, MNRAS, 287, 328
Kümmel, M. W., & Wagner, S. J. 2000, A&A, 353, 867
Lacy, M., Hill, G. J., Kaiser, M. E., & Rawling, S. 1993, MNRAS, 263, 707
Latham, D. 1982, in IAU Colloq. 67, Instrumentation in Astronomy for Large Optical Telescopes, ed. C. M. Humphries (Dordrecht: Reidel), 529
Laurent-Muehleisen, S. A., Kollgaard, R. I., Ciardullo, R., Feigelson, E. D., Brinkmann, W., & Siebert, J. 1998, ApJS, 118, 127
Lawrence, C. R., Zucker, J. R., Readhead, A. C. S., Unwin, S. C., Pearson, T. J., & Xu, W. 1996, ApJS, 107, 541
Lazzati, D., et al. 2001, in Mining the Sky, ed. A. J. Banday, S. Zaroubi, & M. Bartelmann (Berlin: Springer), 501
Loiseau, N. Reich, W., Wielebinski, R. Reich, P., & Muench, W. 1988, A&AS, 75, 67
Maccacaro, T., Wolter, A., McLean, B., Gioia, I. M., Stocke, J. T., Della Ceca, R., Burg, R., & Faccini, R. 1994, Astrophys. Lett. Commun., 29, 1
Mason, K. O., et al. 2000, MNRAS, 311, 456
Massey, P., Strobel, K., Barnes, J. V., & Anderson, E. 1988, ApJ, 328, 315
Mullis, C. R. 2001, Ph.D. thesis, Inst. for Astronomy, Univ. Hawai'i
Mullis, C. R., Henry, J. P., Gioia, I. M., Böhringer, H., Briel, U. G., Voges, W., & Huchra, J. P. 2001, ApJ, 553, L115
Mullis, C. R., et al. 2003, ApJ, 594, 154
Oke, J. B., & Gunn, J. E. 1983, ApJ, 266, 713
Oke, J. B., et al. 1995, PASP, 107, 375
Perlman, E. S., Horner, D. J., Jones, L. R., Scahrf, C., Ebeling, H., Wegner, G., & Malkan, M. 2002, ApJS, 140, 265
Ponman, T. J., Allen, D. J., Jones, L. R., Merrifield, M., Mc Hardy, I. M., Lehto, H. J., & Luppino, G. A. 1994, Nature, 369, 462
Pravdo, S. H., & Marshall, F. E. 1984, ApJ, 281, 570
Rector, A. T., & Stocke, J. T. 2001, AJ, 122, 565
Rengelink, R. B., Tang, Y., de Bruyn, A. G., Miley, G. K., Bremer, M. N., Roettgering, H. J. A., & Bremer, M. A. R. 1997, A&AS, 124, 259
Romer, A. K., et al. 2000, ApJS, 126, 209
Rosati, P., Della Ceca, R., Norman, C., & Giacconi, R. 1995, ApJ, 445, L11
———. 1998, ApJ, 492, L21
Schneider, D. P., Bahcall, J. N., Gunn, J. E., & Dressler, A. 1992, AJ, 103, 1047
Stark, A. A., Gammie, C. F., & Wilson, R. W. 1992, ApJS, 79, 77
Stickel, M. 1993, A&A, 275, 49
Stickel, M., et al. 1998, A&A, 336, 116
Stocke, J. T., Morris, S. L., Gioia, I. M., Maccacaro, T., Schild, R. E., Wolter, A., Fleming, T. A., & Henry, J. P. 1991, ApJS, 76, 813
Treves, A., et al. 1995, ApJ, 442, 589
Trümper, J. 1983, Adv. Space Res., 27, 1404
Veron-Cetty, M.-P., & Veron, P. 2001, A&A, 374, 92
Vikhlinin, A., McNamara, B. R., Forman, W., Jones, C., Quintana, H., & Hornstrup, A. 1998, ApJ, 502, 558
Vikhlinin, A., McNamara, B. R., Hornstrup, A., Quintana, H., Forman, W., Jones, C., & Way, M. 1999, ApJ, 520, L1
Voges, W., Henry, J. P., Briel, U. G., Böhringer, H., Mullis, C. R., Gioia, I. M., & Huchra, J. P. 2001, ApJ, 553, L119
Voges, W., et al. 1999, A&A, 349, 389
Wainscoat, R. J., Cohen, M., Volk, K., Walker, H. J., & Scwhartz, D. E. 1992, ApJS, 83, 11
White, D. A., Jones, C., & Forman, W. 1997, MNRAS, 292, 419
Wilson, A. G. 1952, Trans. IAU, 8, 335
Wold, M., Lacy, M., Dahle, H., Lilje, P., & Ridgway, S. E. 2002, MNRAS, 335, 1017
Xu, W., Lawrence, C. R., Readhead, A. C. S., & Pearson, T. J. 1994, AJ, 108, 395